MRS Energy & Sustainability (2024) 11:193–218

doi:10.1557/s43581-024-00104-3

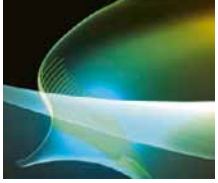

REVIEW

Osmotic power generation based on nanoconfined materials

Lixue Yang, Beijing Institute of Nanoenergy and Nanosystems, Chinese Academy of Sciences, Beijing 101400, China
Shaoxin Li and **Han Qian**, Beijing Institute of Nanoenergy and Nanosystems, Chinese Academy of Sciences, Beijing 101400, China; School of Nanoscience and Technology, University of Chinese Academy of Sciences, Beijing 100049, China
Zhe Wang, School of Chemistry and Life Sciences, Changchun University of Technology, Changchun 130012, China; Advanced Institute of Materials Science, Changchun University of Technology, Changchun 130012, China; Key Laboratory of Advanced Functional Polymer Membrane Materials of Jilin Province, Changchun 130012, China
Zhong Lin Wang, Beijing Institute of Nanoenergy and Nanosystems, Chinese Academy of Sciences, Beijing 101400, China; School of Materials Science and Engineering, Georgia Institute of Technology, Atlanta, GA 30332, USA
Di Wei, Beijing Institute of Nanoenergy and Nanosystems, Chinese Academy of Sciences, Beijing 101400, China; Centre for Photonic Devices and Sensors, University of Cambridge, 9 JJ Thomson Avenue, Cambridge CB3 0FA, UK
Address all correspondence to Zhe Wang at wangzhe@ccut.edu.cn; Zhong Lin Wang at zhong.wang@mse.gatech.edu; Di Wei at dw344@cam.ac.uk

(Received: 13 June 2024; accepted: 25 July 2024; published online: 30 August 2024)

ABSTRACT

The most recent progress in osmotic power generation based on various hierarchically structured materials has been reviewed, analyzing key factors such as surface charge and geometric configuration that could significantly boost both ion selectivity and permeability. Integrating enhanced mass transport from nano-hierarchical structures with improved ion dynamics could herald a new era of highly efficient osmotic power generation.

Realizing the practical application of osmotic power remains a formidable challenge. Despite recent advancements, the feasibility of osmotic power for portable electronics is still uncertain, primarily due to limited power output and portability issues. Enhancing both ion selectivity and permeability is critical for achieving highly efficient osmotic power. Recent advancements with various nanoconfined materials and structures demonstrate significant potential for optimizing these parameters. This review delves into the key factors affecting osmotic power conversion and ion dynamics within nanoconfined structures, including surface charge, geometric configuration, and external stimuli. It systematically examines the applications of one-dimensional, two-dimensional, and three-dimensional nanoconfined materials in osmotic power generation. Hierarchical structures, ubiquitous in natural organisms for efficient mass transport, and ions with distinctive dynamic properties in nanoconfined systems, present opportunities to enhance osmotic power generation efficiency by optimizing pathways for mass transport and ion dynamics. Integrating enhanced mass transport from nano-hierarchical structures with improved ion dynamics could herald a new era of highly efficient osmotic power generation.

Keywords biomimetic · energy storage · environmentally protective · nanostructure · self-assembly

Discussion

Despite the significant challenges of osmotic power in practical applications for portable electronics, recent advancements suggest increasing feasibility through the optimization of various nanoconfined materials with hierarchical structures, particularly in enhancing ion selectivity and permeability simultaneously. The hierarchical structures of these materials and optimized ion dynamics offer potential for efficient unipolar ion transport, paving the way for future highly efficient osmotic power generation.

Introduction

With the progression of global industrialization and urbanization, the significant release of greenhouse gases has emerged as a substantial menace to human health and welfare.[1] To confront this challenge, a pragmatic approach entails the adoption of clean energy as a viable alternative to fossil fuels.[2] Osmotic power, originating from the salinity gradient between freshwater and seawater, embodies sustainable, eco-friendly, and blue energy.[3] Different from pressure-retarded osmosis (PRO), the reverse electrodialysis phenomenon (RED) system can directly convert osmotic power into electrical energy.[4] As a result, the nanoconfined channel-based RED system has gained more attention.[5] In RED systems, the conversion of osmotic power predominantly relies on the selective transport of ions, highlighting the critical advancement of charged nanoconfined channels.[6] These channels can simultaneously exhibit strong selectivity and permeability for ions with opposite charges.[7] Traditional nanochannels, typically exceeding 100 nm in diameter, displayed bulk-free diffusion behavior similar to that in macroscopic liquid systems, where solvated ions moved in opposite directions under the influence of an electric field (Fig. 1a).[8] However, these conventional nanochannel membranes suffer from high membrane resistance, cost inefficiency, and low output power density. In contrast, nanoconfined channels, generally ranging from 2 to 100 nm in diameter, primarily govern ion transport via the electrical double-layer (EDL) (Fig. 1b).[9] Especially in sub-nanoconfined channels (< 2 nm), ion transport will exhibit a range of anomalous behaviors.[10–12] Within such narrow pore systems, the pores themselves carry a charge, and in channels narrower than the Debye length (λ_D), the internal surface charge repels ions of similar charge while attracting ions of opposite charge, thereby serving as primary carriers (Fig. 1c).[13]

Nature offers a unique perspective on "ionic energy" as organisms adapt to their environment, maintain internal stability, and convert energy within cells through ion transport.[14] The electric eel possesses an extraordinary ability to produce powerful electrical discharges.[15] Its electric organ comprises numerous electrocytes, functioning like biological batteries arranged in series along the eel's body to amplify voltage output. To generate an electric current, the eel precisely controls ion dynamics across selectively permeable membranes, establishing a transmembrane ion gradient primarily involving potassium (K^+) and sodium (Na^+) ions. During discharge, specific ion channels and pumps activate, facilitating a rapid influx of Na^+ into the cellular milieu and an efflux of K^+, allowing the cells to achieve a potential of approximately 150 mV (Fig. 2a).[15,16] Additionally, during nerve impulse conduction,[17] the arrival of an action potential at the axon terminals triggers the opening of voltage-gated calcium channels on the presynaptic membrane, allowing calcium ions to flow into the cell. This influx leads to the fusion of synaptic vesicles with the presynaptic membrane, resulting in neurotransmitter release into the synaptic cleft and facilitating communication between neurons (Fig. 2b). Another important example is the variation in neuronal action potentials,[18] primarily driven by differing salinity gradients of Na^+ and K^+ inside and outside the cells. In the quiescent state, extracellular Na^+ concentration surpasses intracellular levels, while intracellular K^+ concentration exceeds extracellular levels. Upon stimulation, sodium channels on the cell membrane open, allowing Na^+ to rapidly enter the cell, raising the internal potential and generating an action potential (Fig. 2c). As shown in Fig. 2d, the kidneys play a crucial role in regulating fluid balance and salt concentration in the body.[19] Within the renal tubules, active transport of Na^+ establishes a salinity gradient, allowing water to passively move from urine back into the bloodstream via osmosis, thereby concentrating urine to reduce water loss. This process requires energy (ATP) to maintain the low concentration of Na^+ within the renal tubule cells, enabling water to flow back into the bloodstream alongside Na^+ via osmotic pressure.

The energy harvesting mechanisms in biological organisms, which rely on ion transportation, demonstrate remarkable efficiency.[20] This raises the question: can we replicate or even surpass nature in harvesting energy through ion transport? The answer is affirmative, thanks to significant advancements in nanomaterial science in recent decades. These advancements have paved the way for fabricating nanochannels from nanoconfined materials with diverse nanostructures.[21] The study of ion transport in such nanoconfined channels is a rapidly growing research field, allowing precise control over channel dimensions at the nano or sub-nano scale.[22] Drawing inspiration from various biological ion channels, a plethora of nanoconfined channels have been engineered utilizing a variety of nanostructures, including one-dimensional (1D) nanopores and nanotubes, two-dimensional (2D) layered membranes, and three-dimensional (3D) self-assembled membranes. These channels have found applications in osmotic power generation.[23] Nanoconfined materials, characterized by distinct nanostructures, exhibit diverse physicochemical properties. This leads to nanoconfined channel membranes with varying ion transport behaviors, consequently resulting in different osmotic power conversion performances.[24] Additionally, the functionalization of nanoconfined materials can modify the physicochemical properties of the nanoconfined channels, thereby altering their osmotic power generation capabilities.[25]

In this review, we focus on addressing the performance deficiencies of nanoconfined materials used in osmotic power generation through meticulous nanostructure design. We introduce and elaborate on two critical factors: ion selectivity and permeability, which influence osmotic power harvesting capabilities. Additionally, we emphasize the dynamic ionic factors impacting osmotic power generation, such as surface charge, geometric structure, and external stimuli, offering insights for optimizing conversion efficiencies. Detailed discussions on osmotic power generation performance across different nanostructures (1D, 2D, and 3D) are provided. Finally, we explore prospective challenges and avenues for future research in nanochannels constructed from nanoconfined materials, leveraging

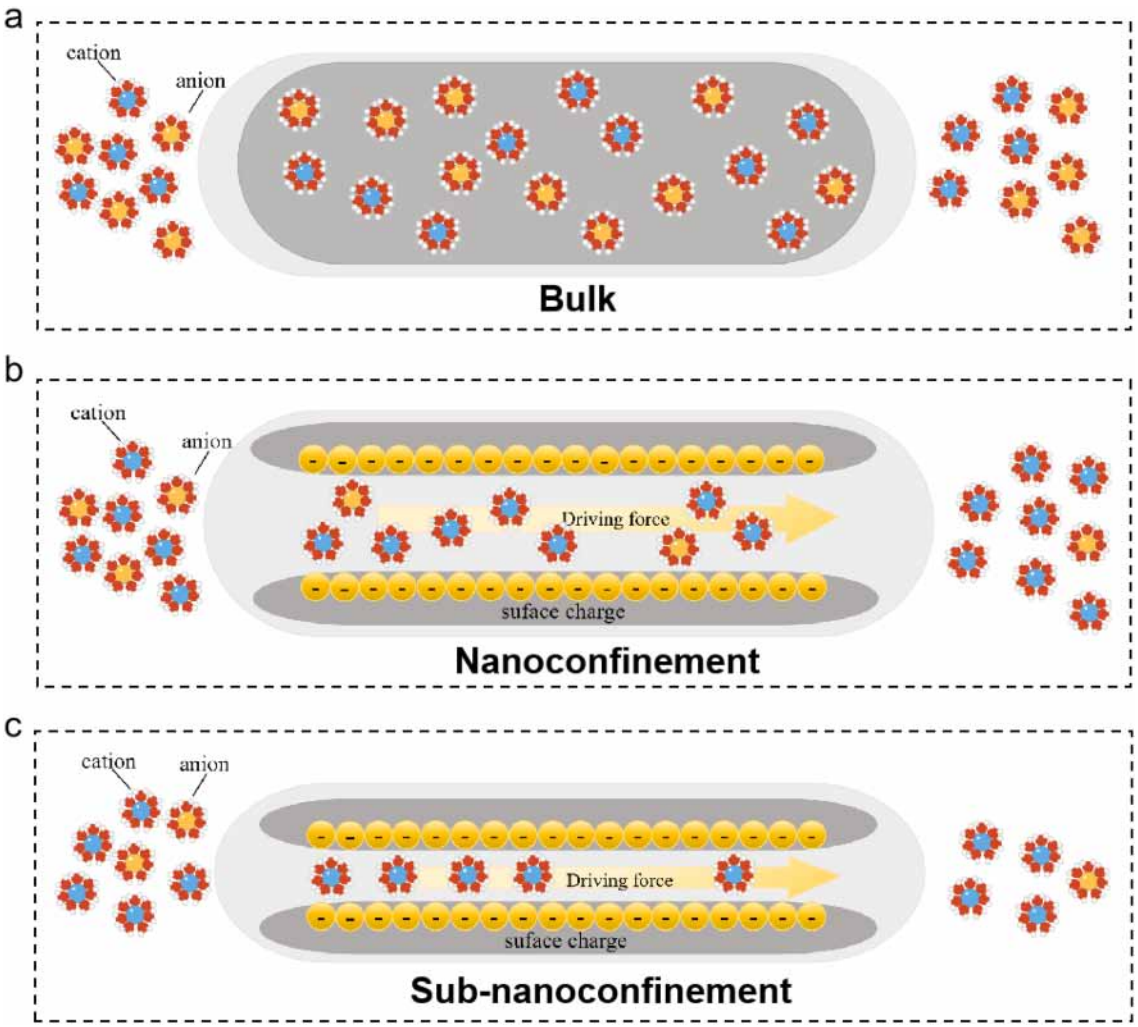

Figure 1. Ion interactions in (a) bulk systems, (b) nanoconfined systems, and (c) sub-nanoconfined systems.

recent progress in optimizing parameters and exploiting unique dynamic characteristics for efficient osmotic power generation.

Ion dynamics in nanoconfined channels

One direct approach to enhancing osmotic power performance involves improving ion selectivity and permeability to achieve more efficient ion transport in environments with salinity gradients.[26] This goal is intricately linked to ion transport at the nanoscale.[27] By adjusting the structure and chemical properties of nanoconfined channels, selective transport of specific ions can be achieved, thereby increasing the efficiency of osmotic power harvesting.[28]

Ion selectivity

A fundamental inquiry regarding nanoconfined channels revolves around understanding the kinetics of ions. In surface-charged nanoconfined channels, ions with opposite charges are preferentially transported, a phenomenon known as unipolar ion transport due to the influence of the EDL, enhancing ion selectivity.[29] On the charged internal surfaces of these channels, electrostatic forces from the EDL prevail, repelling co-ions of similar charge while attracting counter-ions of the opposite charge. Unusual ion transport kinetics have been observed in channels narrower than the Debye length (λ_D) of the electrolyte; surface charges on the inner walls of nanofluidic channels repel like-charged ions and attract counter-ions, making them the dominant charge carriers. The EDL comprises the Stern layer and the diffusion layer, with the characteristic length of the diffusion layer, represented by λ_D, calculable using the Debye–Huckel equation.[30]

$$\lambda_D = \sqrt{\frac{\varepsilon RT}{\sum_{i=1}^{N} F^2 Z_i^2 C_{i,0}}},$$

where ε is the solution permittivity, R is the gas constant, T is the temperature, F is the Faraday constant, N is the total number of ion species, Z_i and $C_{i,0}$ are the valence and bulk concentration of i^{th} ion species, respectively. Graphene oxide (GO),[31] a

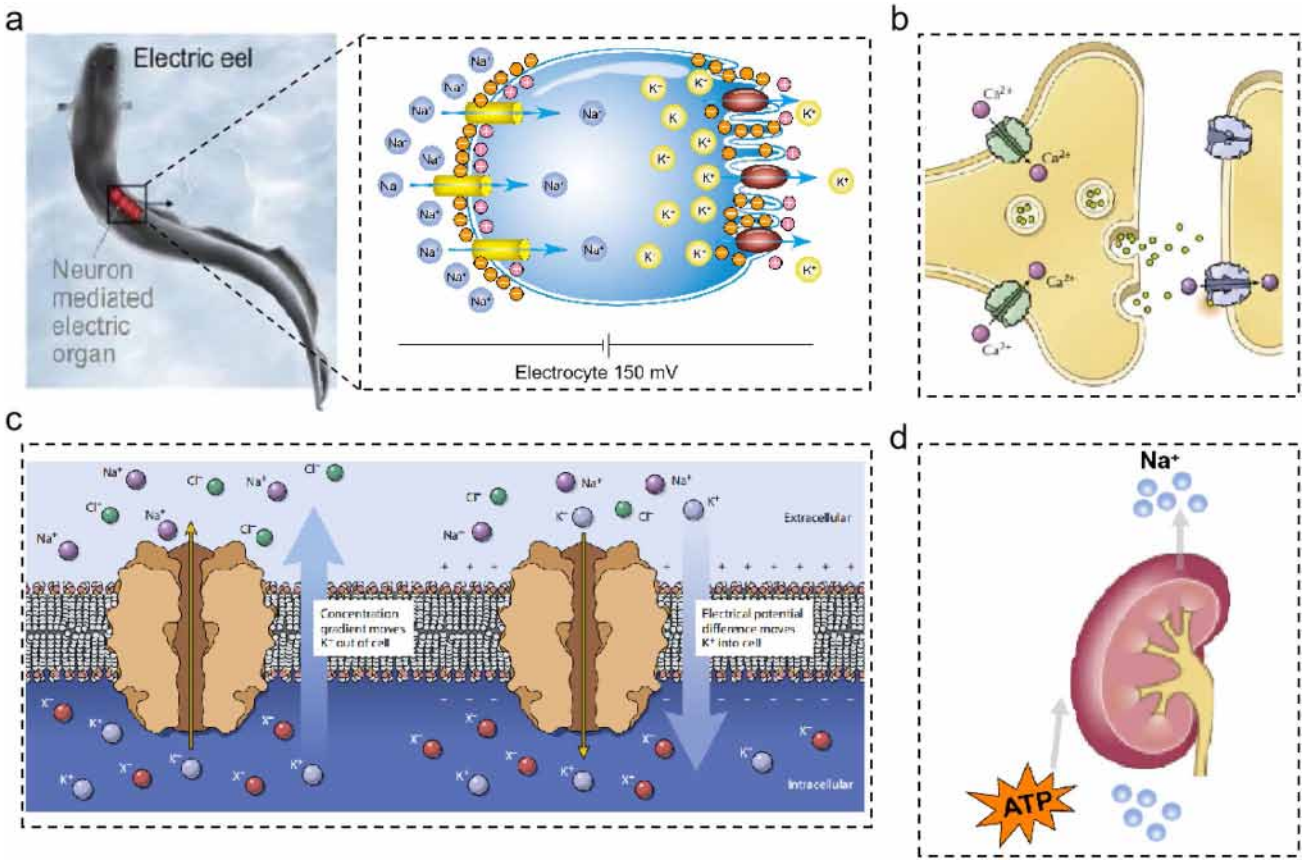

Figure 2. (a) Schematic illustration of the structures of the electric eel's electrocytes and the mechanism of voltage generation in the nanofluidic channel of Na^+ and K^+. Reproduced with permission from Ref. 15. Copyright © 2023 Wiley±VCH GmbH. (b) The process of information transmission and processing by neurons in chemical synapses, (c) The mechanism of action potential generation in neurons, (d) The process of urine concentration in the kidney.

typical 2D nanofluidic material, has been reported to serve as a nanoconfined charging dynamic medium, potentially useful in applications such as ionic analog and voltage gating devices. When the dimensions of the nanofluidic channels are less than 2 nm, the overlapping effects of the EDL, etc. enable unipolar ions to pass through these channels, facilitating observable selective ion transport.[32]

Ion permeability

Employing an interfacial superassembly strategy, a heterostructure membrane comprising orderly arranged mesoporous silica layers (8.2 nm) juxtaposed with macroporous alumina membranes (80 nm) was fabricated. The presence of mesoporous silica layers endows the heterostructure membrane with abundant silanol groups, high specific surface areas, outstanding ion selectivity, and osmotic power conversion capability.[33] Inspired by biological nanochannels, there was growing interest in constructing nanofluidic channel membranes exhibiting diode-like attributes for efficient osmotic power generation.[34] These membranes could be designed by adjusting parameters such as pore size, surface charge, and wettability.[35–37] In nanofluidic devices, current under one voltage polarity surpassed that under the opposite polarity in absolute terms, indicative of diode-like ion transport preferences.[38] For example, deliberate asymmetry in nanofluidic channels,[39] achieved through the careful design of conical nanopores, induced nonlinear ion transport phenomena, thereby directing ion accumulation and depletion under varying voltage conditions and effectively modulating ion flow dynamics. The underlying principle driving this design was the significant enhancement of ion permeability within nanoconfined channels, resulting in more efficient ion transport. In fact, asymmetric designs not only optimized ion permeability but also had particular appeal due to their enormous practical value (water treatment, energy conversion, and biomedical application) in nonlinear ion transport strategies.[40–42]

The Coulomb blockade phenomenon was also observed for ions in nanoconfined structures.[43] When a charged particle attempted to pass through a nanostructure with the same charge, it needed to overcome the potential barrier caused by Coulomb interactions. Nevertheless, when ions passed through nanoconfined channels, the surrounding electric field was restricted, leading to a decrease in ion charge density and thus a weakening of the repulsive forces between ions. Therefore, the Coulomb blockade effect made it easier for ions to pass through nanoconfined channels, thereby enhancing ion permeability.

This seemingly paradoxical phenomenon actually unveiled the potential of harnessing nanoscale effects to control and enhance ion permeability.[44,45] Through the meticulous design of ordered porous membranes, not only could resistance be minimized and output current amplified, but the selective ion transport characteristic of Coulomb blockade could be harnessed to precisely regulate ion passage, thereby enhancing both ion permeability and efficiency.[45] Factors such as surface charge and geometric structure in the design of nanoconfined channel membranes will be further reviewed in subsequent sections.

Nanoconfined materials are used for salinity gradient energy conversion

Materials of varying dimensions, such as 1D nanopores and nanotubes, 2D layered membranes, and 3D self-assembled materials, exhibit unique physical and chemical properties critical to improving osmotic power (Table 1). Factors including surface charge characteristics, stimuli from other physical factors such as temperature and pressure, and geometric structure profoundly impact the output performance. By understanding and harnessing the synergies among these factors, more efficient osmotic power sources tailored to specific materials could be designed. Optimizing material properties in relation to surface charge and structural design enhances the performance of osmotic power generation.[24]

1D nanopore materials

Nanopores and nanotubes were classified as 1D nanopore materials, which were particularly well-suited for studying salinity gradient energy conversion.[11] Their geometric structures and controllable chemical properties enable significant potential for enhancing osmotic power conversion efficiency and regulating selective permeation.[46] By fine-tuning these nanostructures, optimization of ion transport under salinity gradients could be achieved, allowing for efficient energy harvesting. For example, utilizing the ion-track-etched technique to etch polyimide, single conical nanopores were formed, marking the first example of salinity gradient energy conversion using 1D nanopores.[47] In this study, a theoretical framework was proposed to elucidate the electricity generation in nanoporous fluid systems driven by salinity gradients. Computational results indicated that increasing surface charge density and optimizing nanopore sizes enhance cation selectivity when the EDL overlaps within the pore. This framework aligns with the generator mechanism of conventional membrane technology. Experimental evidence showed that the maximum output power from a single nanopore reached approximately 26 pW. Through parallelization, the estimated power density could be increased by one to three orders of magnitude compared to previously used ion exchange membranes. It is worth noting that pH value, geometric structure, and concentration ratio on both sides significantly affected osmotic power performance. Under conditions of pH 10.5, the maximum power obtained from a conical nanopore was approximately 10.9 pW, while in an electrolyte solution with a pH of 3.4, where the nanopore was less charged, the power obtained decreased significantly to 0.6 pW (Fig. 3a). Due to the asymmetric geometric structure of conical nanopores, lower power was generated when the salinity gradient was applied in the reverse direction of the nanopore, as the concentration was lower on the narrow side of the pore. All these effects effectively increased the surface charge density of the nanoconfined channel. As shown in Fig. 3b, significant osmotic power conversion could be measured in single transmembrane boron nitride nanotubes (BNNTs), with the power density reaching 4000 W m^{-2} under a 1000-fold salinity gradient.[48] This was due to the presence of very large pH-sensitive surface charges carried on the inner walls of BNNTs. As the pH increased from 5 to 11, the surface charge density linearly increased from 0.1 to 1 C m^{-2}, the highest value reported to date. Furthermore, this pH-sensitive characteristic had a critical impact on the osmotic transport of the nanotubes, generating osmotic currents due to salinity gradients. Additionally, the authors proposed that this osmotic current differed from the ion-selective mechanism typically assumed in reverse electrodialysis for osmotic power conversion. Instead, it resulted from diffusion osmosis driven by salinity gradients at the interface within the nanotubes. The salinity gradients generated osmotic pressure gradients within the diffusion layer at the interface, with the osmotic pressure drop inside the bilayers being significantly greater than the external pressure drop typically applied. Furthermore, a single-layer molybdenum disulfide (MoS_2) membrane with a uniform pore size of 10 nm and a porosity of 30% achieved a power density of 106 W m^{-2} through parallelization with such nanoporous ion-track-etch membranes, surpassing the results obtained from single boron nitride nanotubes by two to three orders of magnitude and exceeding the power density obtained from classical ion exchange membranes by millions of times.[49] This was because the net diffusion current originates solely from charge separation and concentration distribution within the EDL; thus, it could be expected that in small pores within the overlap range of the EDL, the total current increased more rapidly compared to larger pore sizes. The slight decrease in current at larger pore sizes might be attributed to the reduction in local salinity gradients and the overestimation of the redox potential subtracted. Additionally, molecular-dynamics (MD) simulation further studied the power density generated by the membrane, showing a sharp decrease in power density with increasing layers, indicating that optimal osmotic power generation occurred in the 2D membranes (Fig. 3c).

Nanotubes demonstrated notable capabilities for salinity gradient energy conversion by facilitating the rapid flow of water through hydrophobic single-walled carbon nanotubes, leading to the establishment of structured hydrogen bonds among water molecules. The ordered hydrogen bonded between water molecules and the weak attraction between water and smooth graphene sheets of carbon nanotubes should result in almost frictionless and very rapid flow. For instance, Majumder et al. demonstrated that the velocity of liquid passing through a membrane composed of aligned carbon nanotube arrays was four to five orders of magnitude faster than predicted by traditional fluid flow theories.[50] Furthermore, Cui et al. measured the osmotic

Table 1. Summary of the osmotic power of a nanoconfined channel based on different 1D (italic area), 2D (bold area), and 3D (bold italic area) nanoconfined materials.

Membrane	Modification method	Salinity gradient	Power density	Refs.
Polyimide membrane	*Ion track etching*	*1000 mM/1 mM KCl*	*26 pW*	[47]
BNNTs	±	*1 M/0.001 M KCl*	*4000 W m^{-2}*	[48]
Single-layer MoS_2	±	*10 mM/1 mM KCl*	*106 W m^{-2}*	[49]
DWCNTs	*Photolithography*	*1000 mM/1 mM KCl*	*22.5 kW m^{-2}*	[51]
VMM	**Vertically oriented**	**0.3 M KCl**	**25 mW m^{-2}**	[61]
V-GO	**Vertically oriented**	**0.5 M/0.01 M NaCl**	**10.6 W m^{-2}**	[62]
GOM	**Oppositely charged GO pairs**	**0.5 M/0.01 M NaCl**	**0.77 W m^{-2}**	[63]
MXMs	**Oppositely charged MXene pairs**	**0.5 M/0.01 M NaCl**	**4.6 W m^{-2}**	[64]
BHMXM	**Vertically oriented oppositely charged MXene pairs**	**0.5 M/0.01 M NaCl**	**8.6 W m^{-2}**	[65]
GO/CNFs	**Assembled with nanoconfined materials (CNFs)**	**0.5 M/0.01 M NaCl**	**4.19 W m^{-2}**	[66]
GDP	**Assembled with nanoconfined materials(DODAB + PAAS)**	**0.5 M/0.01 M NaCl**	**13.38 W m^{-2}**	[67]
MXene/PBONF-50	**Assembled with nanoconfined materials (PBONF)**	**0.5 M/0.01 M NaCl**	**15.7 W m^{-2}**	[68]
VGO	**Interface redox reactions**	**±**	**15,900 W m^{-2}**	[76]
V-NbP	**Introducing phosphorus vacancies**	**Natural Australian Seawater/ River water**	**10.7 W m^{-2}**	[79]
PVMs	**Introducing planar nanopores**	**1 M/1 mM KCl**	**10.9 W m^{-2}**	[80]
SAMM@AAO	***Assembled with nanoconfined materials (AAO)***	***1000 mM/10 mM NaCl***	***6.76 W m^{-2}***	[93]
SP-MIL-53	***Assembled with nanoconfined materials (SP)***	***0.5 M/0.01 M KCl***	***8.3 W m^{-2}***	[94]
UIO-66-NH_2 (PSS)/ZIF-8 (PVP)	***Assembled with nanoconfined materials (MOF-on-MOF)***	***5 M/0.01 M NaCl***	***40.1 W m^{-2}***	[95]

Table 1. (continued)

Membrane	Modification method	Salinity gradient	Power density	Refs.
COF-LZU1@CNT-CNF	*Assembled with nanoconfined materials (CNT-CNF)*	*Natural seawater/River water*	*4.26 W m^{-2}*	[97]
PyPa-SO$_3$H/SANF	*Assembled with nanoconfined materials (SANF)*	*Real seawater/River water*	*9.6 W m^{-2}*	[98]
TpEB@TpPa-SO$_3$Na	*Asymmertric geometry*	*0.5 M/0.01 M NaI*	*210.1 W m^{-2}*	[99]
COF-(SO$_3$Na)$_x$/PAN	*Introducing thermosensitive organic ligands*	*0.5 M/0.01 M NaCl*	*97 W m^{-2}*	[100]

power conversion of individual double-walled carbon nanotubes (DWCNTs) with an inner diameter of 2.3 nm and a length of 100 μm.[51] Through the fabrication of nanopore devices using photolithography, a high power density of up to 22.5 kW m^{-2} was recorded, surpassing pristine graphene (1.5 kW m^{-2}) by a factor of 15 and MoS_2 nanopores (106 W m^{-2}) by a factor of 30. However, due to the inverse relationship between power density and the length of the tube or channel, the length of MoS_2 nanopores was 0.6 nm, while the length of DWCNTs measured here was 100 μm, yielding the highest unit length power density. The reason for DWCNTs having such high power density might lie in the ultra-low friction at the water–solid interface with slip lengths up to several micrometers (Fig. 3d).

1D nanoconfined channels, with their distinctive geometric features and size effects, provided the advantage of precise fabrication and control, essential for optimizing the performance of salinity gradient energy conversion systems. These nanoconfined channels, through their nanostructured design, could precisely control ion transport behavior, thereby maximizing osmotic power conversion efficiency.[52,53] For instance, by combining cone-shaped solid-state synthesized polyimide nanochannels with chloride-responsive molecules, a biomimetic Cl^- nanochannelcapable of switching its state in response to voltage was developed.[54] In the nanoconfined channel, chloride-responsive molecules were initially immobilized on the inner walls of the nanochannel via conventional 1-ethyl-3-(3-dimethylaminopropyl) carbodiimide (EDC)/N-hydroxysuccinimide (NHSS) chemistry, keeping the channel closed in the absence of Cl^-. Upon addition of Cl^- and their binding to the responsive molecules within the channel, a charge change occurred, repelling anions and causing the channel to open. Subsequently, under applied voltage, Cl^- was released from the responsive molecules, returning the channel to its closed state. This system not only enabled efficient selective transport of Cl^- but also allowed precise modulation of channel states through voltage control (Fig. 3e). Additionally, utilizing ion track etching techniques to etch polyethylene terephthalate (PET), funnel-shaped nanoconfined channels were formed, with carboxyl ester groups formed on the inner surface of the channels to achieve controllable ion transport.[39] Funnel-shaped nanoconfined channels exhibited different ion transport properties from cylindrical and conical nanoconfined channels, particularly with their switchable ion selectivity. In negatively charged funnel-shaped nanoconfined channels, due to the preferential movement of cations from tip to base via a rocking ratchet mechanism, the channel exhibited high conductivity under a negative voltage and low conductivity under a positive voltage. Furthermore, funnel-shaped nanoconfined channels containing negatively charged cone-like segments and electrically neutral cylindrical segments might reverse ion flow direction under positive voltage, as under positive voltage, the cations in the cone-shaped segments concentrated near the electrically neutral cylindrical segments, maintaining a high current state, whereas under negative voltage, cations were more likely to leave these regions, resulting in reduced current. This structure endows funnel-shaped nanoconfined channels with complex and efficient regulation capabilities in selective ion transport and voltage response (Fig. 3f). Despite the advantages of 1D nanoconfined pores, such as high ion selectivity, ion permeability, high-output power density (22.5 kW m^{-2}) (Fig. 10a), and tunable structure, such systems often face challenges such as power density calculations based on impractical cross-sectional areas, complex manufacturing processes, being hard to scale-up, and high costs. Therefore, researchers have begun to focus on 2D layered membranes, which might offer more practical and cost-effective alternatives to address the limitations of 1D nanoconfined pores in osmotic power practical applications.[55]

2D layered membranes

2D layered membranes offer several notable advantages, making them valuable in various applications. Firstly, these nanostructured membranes possess a larger specific surface area, providing more active sites and increasing the area for ion exchange, thereby significantly enhancing their performance. Secondly, their surfaces are easily modifiable and functionalized, allowing precise adjustment of their electrochemical activity and

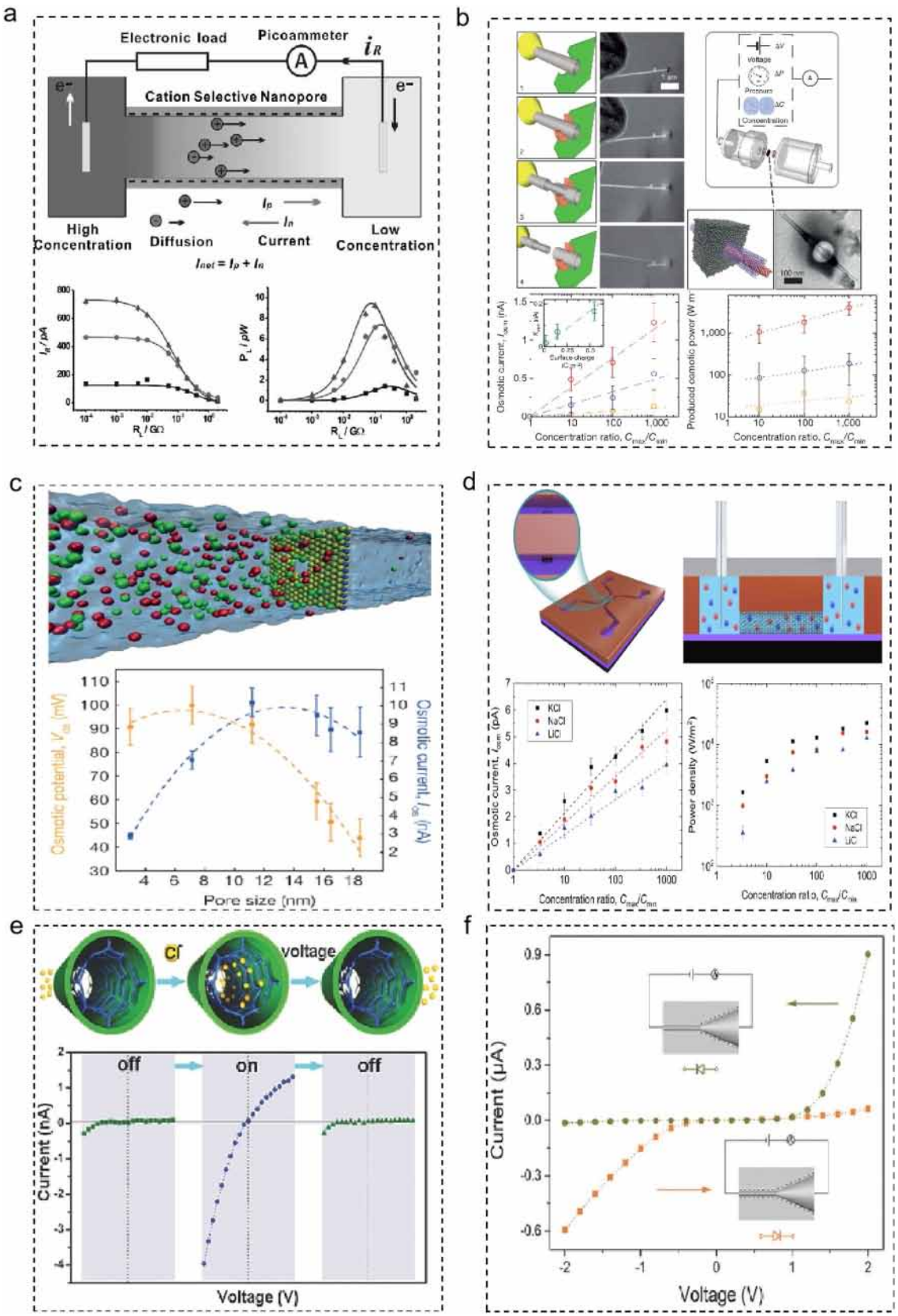
a
Electronic load
Picoammeter
i_R
Cation Selective Nanopore
e⁻
e⁻
High Concentration
Diffusion
I_p
I_n
Current
Low Concentration
$I_{net} = I_p + I_n$
I_R / pA
R_L / GΩ
P_L / pW
R_L / GΩ
b
Voltage
Pressure
Concentration
100 nm
Osmotic current, I_{osm} (nA)
Surface charge (C m⁻²)
Concentration ratio, C_{mid}/C_{min}
Produced osmotic power (W m⁻²)
Concentration ratio, C_{mid}/C_{min}
c
Osmotic potential, V_{os} (mV)
Osmotic current, I_{os} (nA)
Pore size (nm)
d
KCl
NaCl
LiCl
Osmotic current, I_{osm} (pA)
Concentration ratio, C_{mid}/C_{min}
Power density (W/m²)
Concentration ratio, C_{mid}/C_{min}
e
Cl⁻
voltage
off
on
off
Current (nA)
Voltage (V)
f
Current (μA)
Voltage (V)

◂**Figure 3.** (a) Schematic illustration of the net diffusion current generation and electrical power output from a single nanopore to supply R_L. Reproduced with permission from Ref. 47. Copyright © 2010 WILEY-VCH Verlag GmbH & Co. KGaA, Weinheim. (b) Hierarchical single nanotube set-up and osmotic power generation under salinity gradients. Reproduced with permission from Ref. 48. Copyright © 2013, Springer Nature. (c) A typical simulation box used in molecular-dynamics simulations and the osmotic potential and current as a function of pore size. Reproduced with permission from Ref. 49. Copyright © 2016, Springer Nature. (d) The single CNT device and the osmotic power generation under salinity gradients. Reproduced with permission from Ref. 51. Copyright © 2023, Springer Nature. (e) Biomimetic voltage-gated chloride nanoconfined channel and responsive switchability of the (AIPA-BBA)-modified nanoconfined channel after reversible activation with Cl^-. Reproduced with permission from Ref. 54. Copyright © 2016 WILEY-VCH Verlag GmbH & Co. KGaA, Weinheim. (f) Anomalous ionic transport properties of the funnel-shaped nanoconfined channel with a negatively charged conical segment and an electro-neutral cylindrical segment. Reproduced with permission from Ref. 39. Copyright © 2016 WILEY-VCH Verlag GmbH & Co. KGaA, Weinheim.

ion selectivity, particularly in fields such as osmotic power generation.[56,57] Additionally, 2D layered membranes exhibit excellent mechanical and chemical stability, ensuring durability during use and stable operation under harsh environmental conditions, thus broadening their range of applications. It's noteworthy that the interlayer spacing of these membranes is adjustable, enabling the formation of nanoconfined channels with higher ion flux, further enhancing their performance. Finally, the construction of 2D nanoconfined channels is relatively simple and cost-effective, facilitating industrial production and scale-up for practical applications.[58–60] Therefore, 2D layered membranes hold significant potential for increasing power density and scaling up applications. Overall, these advantages collectively underscore the pivotal role and extensive application prospects of 2D layered membranes in osmotic power.

In 2D nanoconfined channels, efficient ion transport primarily occurred within the size of λ_D. Recently, some experimental observations indicated that unidirectional interlayer pathways in vertically oriented 2D layered structures along channels conferred ultrafast ion transport, significantly outperforming their counterparts composed of horizontally stacked structures. For instance, vertically oriented MXene (VMM) membranes offered ultrafast ion permeation rates through their oriented pathways, exhibiting approximately 1000-fold higher ion permeation rates compared to horizontally stacked MXene (HMM) membranes.[61] This notable performance difference was primarily attributed to the straight and penetrating channel structures in VMM membranes, allowing for shorter ion migration distances, whereas in HMM membranes, ions must traverse along zigzag paths through interlayer gaps, resulting in significantly increased travel distances, far exceeding the straight shortest distance. Additionally, the surface of VMM membranes featured a larger effective inlet area, combined with lower energy losses during ion migration, collectively contributing to their ability to achieve substantial current density of up to 8.17 A m^{-2} and output power density of 25 mW m^{-2} in electrolyte solution and gas pressure environments (Fig. 4a). Just as MXene membranes with vertical nanoconfined channels demonstrated outstanding ion permeability performance, vertically transmitting graphene oxide (V-GO) membranes also exhibited excellent osmotic power conversion performance. According to Zhang et al., this V-GO membrane demonstrated superior ion selectivity and ion permeability, with performance three orders of magnitude higher than horizontally transmitting H-GO membranes.[62] This enabled V-GO to achieve an unprecedented output power density of up to 10.6 W m^{-2} under conditions of mixed seawater and river water. Furthermore, by adjusting the salinity gradient and pH value of the electrolyte solution, the power density of V-GO could be further increased to 34 W m^{-2}, significantly surpassing MXene membranes (21 W m^{-2}) under the same conditions. Through theoretical analysis and MD simulation, researchers have elucidated the mechanism of ultrafast ion transport in V-GO (Fig. 4b).

Moreover, combining asymmetric charges within geometric structures could effectively reduce energy dissipation and further improve osmotic power generation. Introducing asymmetric charge distribution in 2D layered membranes could guide directional ion movement within channels, minimizing energy loss. This combination maximized the utilization of ion kinetic energy, achieving efficient energy harvesting and providing crucial technical support for applications in osmotic power and related fields. For instance, Ji et al. reported a nanostructured reverse electrodialysis system based on 2D materials, including cascaded vertical nanochannels in graphene oxide (GO) membranes, for efficient osmotic power conversion.[63] By pre-assembly modification, the surface charge polarity of 2D nanochannels could be effectively adjusted, resulting in highly cationic or anionic selective. This complementary bidirectional ion diffusion process led to effective charge separation, forming superimposed electrochemical potentials and ion fluxes. By adjusting the ratio of mixed high concentration (0.5 M) and low concentration (0.01 M) ion solutions, a high-output power density of 0.77 W m^{-2} was achieved, and the serially alternating use of GO pairs could also generate up to 2.7 V of voltage to meet the energy demands of electronic devices. Additionally, combining MXene with asymmetric charges could further enhance osmotic power performance (Fig. 5a). As shown in Fig. 5b, Li et al. reported a high-performance osmotic power generation technology combining oppositely charged $Ti_3C_2T_x$ MXene membranes (MXMs) with enclosed horizontal 2D nanofluidic channels.[64] These 2D MXene nanoconfined channels with negative or positive charges exhibited typical surface charge-controlled ion transport characteristics and demonstrated excellent cationic or anionic selectivity. By mixing artificial seawater (0.5 M NaCl) and river water (0.01 M NaCl), they achieved a maximum power density of approximately 4.6 W m^{-2}, and by serially connecting ten MXM-RED stacks, they achieved an output voltage of 1.66 V, directly providing power for electronic devices. In the preceding paragraph, we summarized that the ion transport rate of vertically oriented 2D nanoconfined channels was higher than that of their horizontally oriented counterparts. Furthermore, Li et al. prepared a vertically oriented biomimetic heterostructured

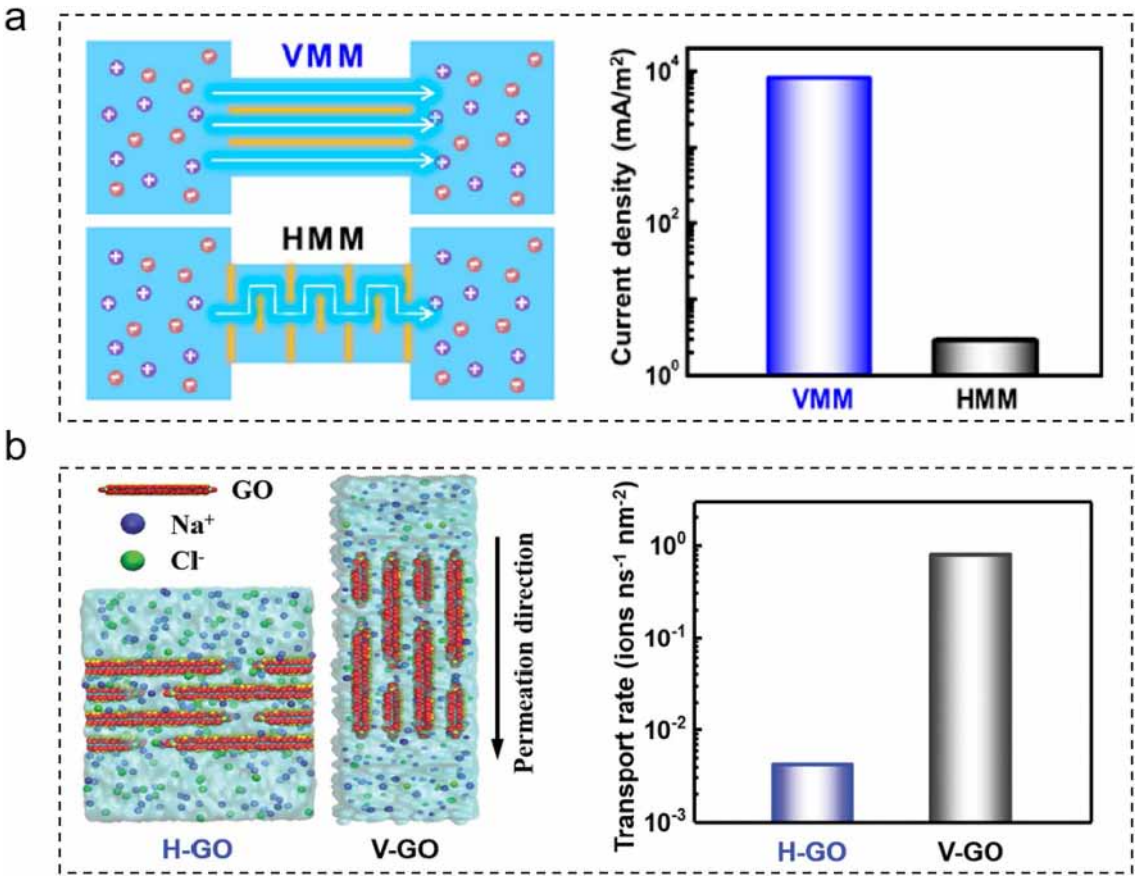

Figure 4. (a) Schematic of ion transport in HMMs and VMMs and the current density driven by hydraulic pressure. Reproduced with permission from Ref. 61. Copyright © 2020, American Chemical Society. (b) The MD simulation of the H-GO or V-GO (right) and the transport rate of Na^+ ions. Reproduced with permission from Ref. 62. Copyright © 2020, WILEY-VCH Verlag GmbH & Co. KGaA, Weinheim.

$Ti_3C_2T_x$ MXene membrane, composed of positively charged MXene (PCM) layers and negatively charged MXene (NCM) layers, with a high rectification current (rectification ratio up to 15.4), demonstrating its potential utility in reverse electrodialysis osmotic power conversion.[65] Under the salinity gradient of synthetic seawater and river water, the power density reached 8.6 $W\,m^{-2}$, and under a 500-fold salinity gradient, the power density reached 17.8 $W\,m^{-2}$ (Fig. 5c).

Moreover, an effective approach to enhancing osmotic power conversion performance involves composite formation by integrating other nanoconfined materials with 2D layered membranes, resulting in the creation of unique nanoconfined channels. This strategy enables the exploitation of the distinctive properties of various materials. Through the integration of diverse nanomaterials, composite membranes with tailored pore structures and functionalized interfaces can be designed, facilitating faster and more efficient ion transport. For example, Wu et al. proposed a clever technique that involved assembling GO nanosheets with cellulose nanofibers (CNFs) to enhance ion transport limitations and achieve efficient osmotic power conversion. CNFs, being prevalent natural nanomaterials, exhibited highly anisotropic characteristics and possessed abundant functional group density.[66] The resulting assembled membrane not only enlarges existing narrow channels, thus reducing energy barriers for ion transport, but also introduces spatial charges between GO nanosheets to maintain ion selectivity. Benefiting from the effective assembly of GO with CNFs, a power density of 4.19 $W\,m^{-2}$ was achieved by mixing artificial seawater and river water. By increasing the solution temperature, the power density was raised to 7.20 Wm^{-2} (Fig. 6a). Wang et al. proposed an ion-selective membrane based on GO, synergistically enhanced through modification with ion polymers and amphiphilic molecules, to enhance membrane permeability and selectivity.[67] The ion polymer sodium polyacrylate (PAAS) brought negative charge groups to the nanochannels, while the amphiphilic molecule dimethyldioctadecylammonium bromide (DODAB) adsorbed more PAAS molecules, enhancing ion selectivity and forming a hydrophobic interface within the nanochannels to reduce ion transport resistance. Therefore, compared to GO/PAAS (GP) membranes, GO/DODAB/PAAS (GDP) membranes exhibited higher ion selectivity and permeability. A permeation-type generator equipped with GDP membranes demonstrated up to 32% energy conversion efficiency under a 50-fold salinity gradient. Under salinity gradients of real river water and seawater,

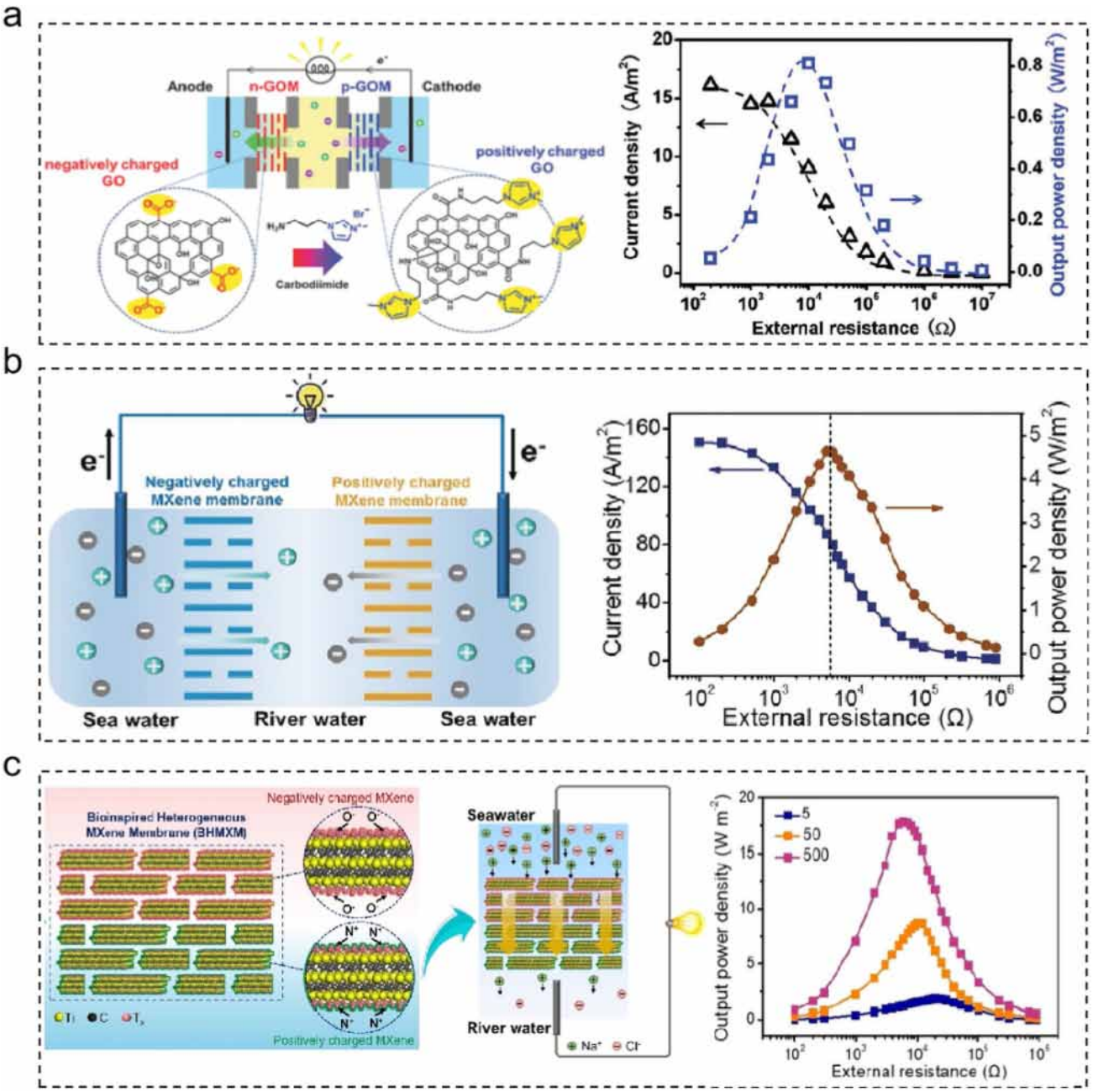

Figure 5. (a) Schematic diagram of the device integrated with osmotic power generation using positively and negatively charged GO pairs and the harvested osmotic power. Reproduced with permission from Ref. 63. Copyright © 2016 WILEY-VCH Verlag GmbH & Co. KGaA, Weinheim. (b) Scheme of the MXM-based nanofluidic energy harvesting device and the current density and output power density of the MXM-RED. Reproduced with permission from Ref. 64. Copyright © 2020 WILEY-VCH Verlag GmbH & Co. KGaA, Weinheim. (c) Illustration of the osmotic power conversion based on the bioinspired BHMXM and the output power density of a BHMXM. Reproduced with permission from Ref. 65. Copyright © 2020 Wiley-VCH GmbH.

the generator achieved a maximum power density of 13.38 W m^{-2} (Fig. 6b).

Moreover, Duan et al. successfully constructed a heterogeneous structured membrane by combining the layered channels of MXene layers with nanoscale poly (benzimidazole) nanofibers (PBONF) through a step-by-step filtration method.[68] This MXene/PBONF-50 heterogeneous membrane exhibited excellent mechanical properties (strength up to 221.6 MPa, strain of 3.2%), high ion selectivity (up to 0.87), and remarkable output power density (up to 15.7 W m^{-2}) under a 50-fold salinity gradient. Excitingly, even on a larger test area of 0.79 mm^2, the heterogeneous membrane still demonstrated a high power density of 6.8 W m^{-2} and long-term stability (Fig. 6c). The combination of 2D GO, known for its high flexibility and abundant surface charges, with layered MXene materials presents an enticing opportunity for composite membrane fabrication, rendering

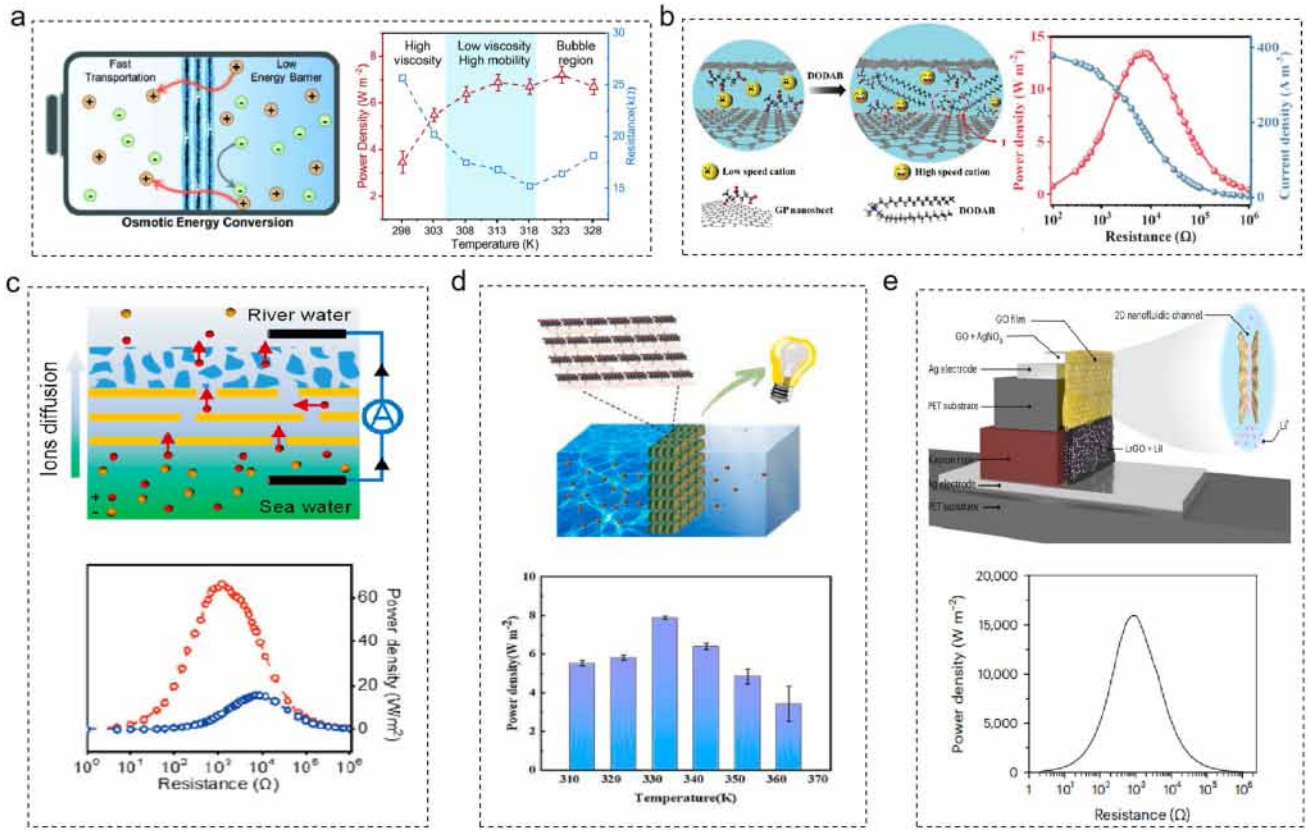

Figure 6. (a) Osmotic power harvesting system and thermal dependence of osmotic power conversion. Reproduced with permission from Ref. 66. Copyright © 2020 The Royal Society of Chemistry. (b) Schematic diagram of the GO-based laminate membrane for osmotic power conversion and the osmotic power harvesting of GDP membrane. Reproduced with permission from Ref. 67. Copyright © 2023 Wiley-VCH GmbH. (c) Schematic diagram of the device for capturing osmotic power and the output power density of the MXene/PBONF-50 heterogeneous membrane. Reproduced with permission from Ref. 68. Copyright © 2023, American Chemical Society. (d) Schematic of the transmembrane ionic transport and the effect of the temperature of the solution on the power density of the MXene/GO-6 composite membrane. Reproduced with permission from Ref. 70. Copyright © 2022 Published by Elsevier B.V. (e) Schematic illustration of the 2D nanofluidic channels and the output power density as a function of the electronic load resistance. Reproduced with permission from 76. Copyright © 2024 Springer Nature.

them prime candidates for energy conversion applications owing to their high surface charge density and well-defined transport channels.[69] Through the incorporation of GO nanosheets into MXene membranes, hydrogen bonding arises between the carboxyl groups of GO and the adjacent hydroxyl end groups of MXene, enhancing their adhesion and thereby bolstering the mechanical strength of the membrane. Fine-tuning the content of GO within the composite membrane enables optimization of the device's output current and voltage, ultimately leading to higher output power density. At room temperature (298 K), the output power density reached approximately 3.7 W m^{-2} by mixing artificial river water and seawater.[70] With the temperature increased to 333 K, the power density could be further increased by twofold, reaching up to 7.88 W m^{-2}. By controlling the appropriate ratio between GO and MXene, excellent voltage-gated ion transport behavior can be achieved (Fig. 6d). For instance, Ouyang et al. proposed a strategy for preparing layered MXene-GO membranes using a vacuum filtration method, resulting in layered 2D MXene-GO membranes (MGOm) with excellent conductivity and chemical stability, achieving outstanding voltage-gated ion transport performance.[71] The channels within the membrane, containing charges or dipoles, facilitate the movement of electrons or dipoles under the influence of membrane potential. By modulating the transmembrane potential, the transition between closed and open states of voltage-gated ion channels can be regulated. The application of a negative potential enhances the interaction force between charged MGOm sheets and cations (K^+) under osmotic pressure, thereby promoting ion permeability. Conversely, a positive potential weakens electrostatic attraction, leading to reduced ion permeability. Moreover, investigations have highlighted the impact of MXene and GO on voltage-gated ion transport at various modulation ratios, with optimal ion permeability achieved at a MXene modulation ratio of 7:3.

In addition, chemically built-in electric fields could be introduced through interface redox reactions to significantly enhance the energy density of devices and affect the diffusion kinetics of ions in nanoconfined spaces.[72,73] For example, Peng et al.

developed an ultrathin (approximately 10.5 μm) solid-state high power ion–electron source, implementing fractal geometry space-filling curves (Peano and Hilbert curves) to maximize length while occupying minimal area.[74,75] Power and energy density were enhanced for practicality, achieving an energy density of about 1.4 kWh m^{-2} and a power density of 16.07 kW m^{-2}. They successfully achieved this technological breakthrough by combining carefully controlled Ag/Ag redox reactions with efficient cation transport in horizontal nanoconfined channels of GO. Inspired by the efficient ion transport kinetics within the GO 2D nanofluidic channels and customized interface redox reactions, Yang et al. designed a vertical GO 2D nanofluidic channel based on permeation effects and electrode redox reactions, achieving an ultra-high-output power density of 15,900 W m^{-2} (Fig. 6e).[76] Moreover, portable energy harvesting devices were realized based on efficient ion transport within 2D nanofluidic channels driven by humidity. Yang et al. demonstrated an ultrathin (approximately 10 μm) osmotic power source based on 2D nanofluidic GO material with a volumetric-specific energy density of 6 mWh cm^{-3} and a power density of 28 mW cm^{-3}. By utilizing 3D aerogel structures, the areal power density was increased to 1.3 mW cm^{-2}. These devices are capable of operating at -40 °C and overcoming humidity limitations (Fig. 6e). Furthermore, these devices achieve a thickness of approximately 10 μm, can be printed on various insulating substrates like paper, plastic, or fabric, operate at room temperature without organic electrolytes, and exhibit minimal self-discharge when vacuum-sealed.[14] Integration of printable circuits and energy management systems (paper-based TENG and osmotic energy storage) on a single sheet of paper enabled in-situ conveyance of crucial physiological parameters, including body temperature, etc.[77,78]

Recent studies have demonstrated that introducing vacancies in 2D materials could effectively enhance their osmotic power conversion performance as well. This strategy increases the negative surface charge of the material, thereby accelerating the migration speed of ions across the membrane and enhancing ion selectivity. Practical tests have revealed that 2D nanomembranes with vacancy introduction achieve remarkable power density in osmotic power generators, surpassing existing commercial standards. For example, the introduction of phosphorus vacancies in niobium oxyphosphate ($NbOPO_4$) nanosheets significantly increases the negative surface charge of the 2D nanoconfined membrane, facilitating rapid transmembrane ion migration and high ion selectivity.[79] When applied to natural seawater and river water, a power density of up to 10.7 W m^{-2} was achieved, far exceeding the commercial benchmark of 5.0 W m^{-2} (Fig. 7a). Furthermore, meticulously engineered porous structures can effectively enhance membrane permeation performance, leading to more efficient osmotic power conversion. Introducing planar nanopores on zeolite nanosheets not only reduces the tortuous path of ion diffusion but also provides additional vertical ion channels, significantly boosting transmembrane ion flux.[80] The restricted interlayer spacing serves as a selective barrier, enhancing ion selectivity. Processing a 1000-fold salinity gradient, porous zeolite membranes exhibit a 16-fold increase in output power density compared to their non-porous counterparts, reaching up to 10.9 W m^{-2} (Fig. 7b). While 2D layered membranes offer potential for scale-up applications owing to their high specific surface area, they face significant limitations due to transmembrane resistance. This resistance imposes tortuous paths for ion diffusion through the membrane, resulting in energy loss and decreased efficiency. Moreover, these membranes exhibit limited ion selectivity and insufficient permeability, constraining their widespread use in osmotic power applications (Fig. 10b).[81] Therefore, despite having certain advantages, 2D layered membranes still face challenges when confronted with these issues, requiring the exploration of more effective solutions. In contrast to 2D nanoconfined materials, 3D nanoconfined materials offer larger volumes and a more diverse array of channel structures, potentially increasing ion flux and enabling high-selectivity filtration of specific ion types.[82] Therefore, the introduction of 3D nanostructured materials is anticipated to address some of the limitations of 2D nanoconfined materials and open new avenues for the advancement of osmotic power conversion technologies.

3D self-assembled membrane

In comparison to 2D nanoconfined materials, 3D nanoconfined materials offer substantial advantages in the realm of osmotic power. Firstly, their larger volume and more abundant channel structures afford greater ion accommodation and provide extensive pathways for ion transport, resulting in heightened ion flux. This augmented flux suggests the potential for higher energy output in osmotic power conversion systems.[83] Secondly, the precisely engineered channel structures of 3D nanoconfined materials enable high-selectivity filtration for specific ion types, which is essential for enhancing system efficiency and purity.[84] Moreover, 3D structures typically exhibit stronger structural stability, ensuring sustained performance over prolonged periods and under diverse environmental conditions, thereby enhancing system longevity and stability. Crucially, in addressing the scalability challenges of RED systems, 3D self-assembled membranes are poised to emerge as a principal avenue for developing streamlined, efficient, and high power density osmotic devices.[85]

3D self-assembled membranes, characterized by high pore density and nanoscale pores, hold significant promise for osmotic power applications.[86–88] Among these, metal–organic frameworks (MOFs) stand out as exceptional candidates for osmotic power conversion. These materials boast immense surface area and intricate pore structures, providing optimal conditions for molecular adsorption and diffusion, thereby augmenting osmotic process efficiency. Their high tunability enables precise control over osmotic performance by adjusting structure and composition.[89] Moreover, MOFs exhibit outstanding chemical stability and mechanical strength, ensuring stable operation across diverse environmental conditions.[90] However, due to MOFs' relatively low surface charge density, the introduction of specific functional groups can enhance ion selectivity in nanoconfined membranes, further optimizing their performance in osmotic power conversion.[91] For instance, the

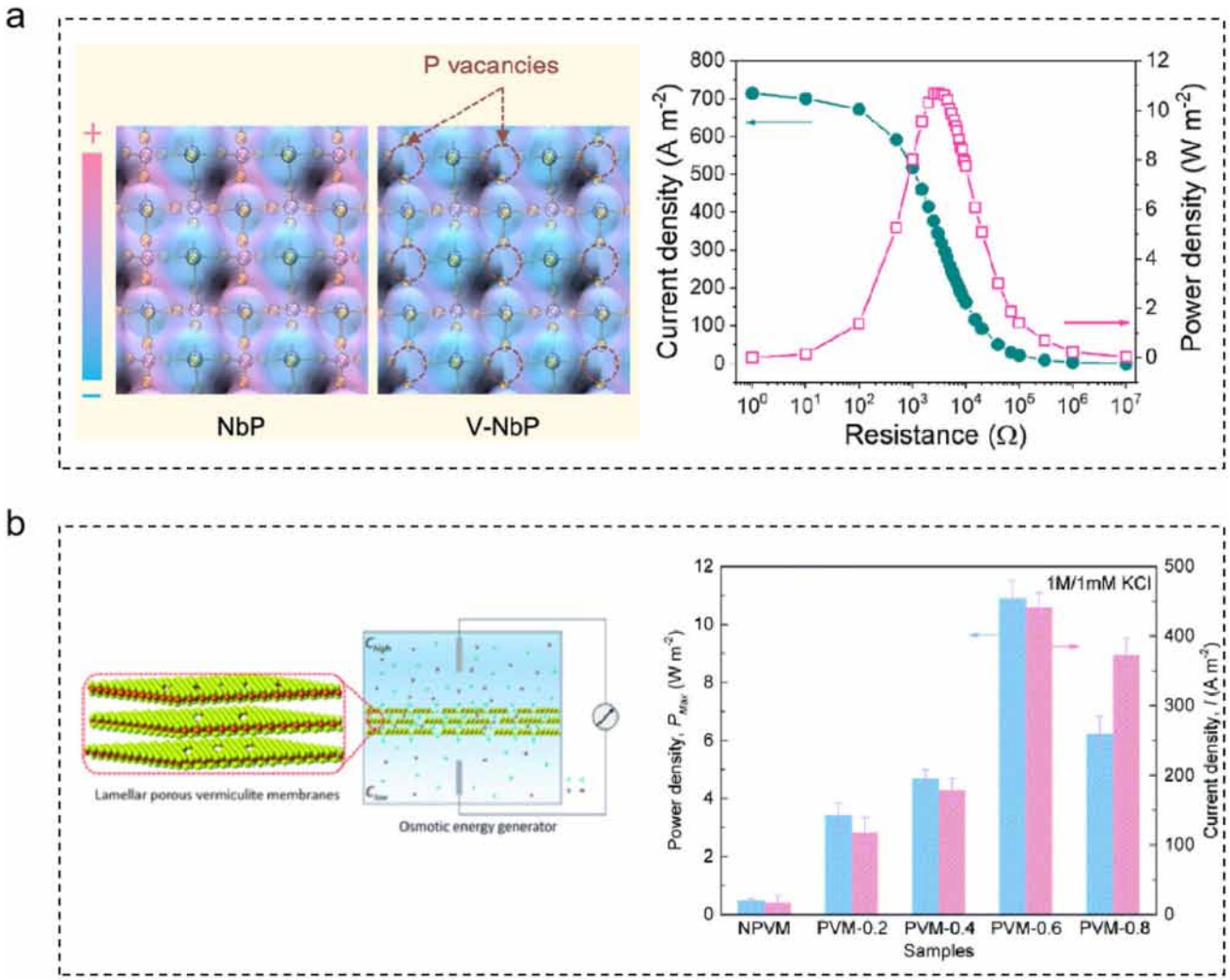

Figure 7. (a) DFT calculations and the osmotic power conversion of V-NbP membranes under a salinity gradient of 0.5 M l 0.01 M NaCl. Reproduced with permission from Ref. 79. Copyright © 2023, American Chemical Society. (b) Schematic representation of the experimental set-up and power and current density for PVMs under a 1 M/1 mM KCl salinity gradient. Reproduced with permission from Ref. 80. Copyright © 2021, The Royal Society of Chemistry.

incorporation of 2,2,6,6-tetramethylpiperidine-1-oxyl (TEMPO) into MOFs enhances the presence of oxygen-containing functional groups within nanochannels, thus enlarging their size and augmenting the ion selectivity and energy conversion efficiency of nanoconfined membranes. Fu et al. achieved this by developing a nanofluidic mixed membrane composed of TEMPO-oxidized cellulose nanofibers (T-CNF) and manganese-based MOFs via a straightforward in-situ synthesis method.[92] The introduction of T-CNF enabled the MOF/T-CNF mixed membrane to demonstrate a remarkable cation selectivity of up to 0.93. Within the 3D interconnected nanochannels, MOFs provided abundant transmission pathways for ions. The resultant MOF/T-CNF mixed membrane exhibited a high ion flux through the membrane and a low ion permeation energy barrier, closely associated with its exceptional energy conversion efficiency of up to 36%. When subjected to a 50-fold salinity gradient between simulated seawater and river water, the MOF/T-CNF mixed membrane achieved an impressive maximum power density of 1.87 W m^{-2}, representing a fivefold increase in output power density compared to pure T-CNF membranes (Fig. 8a). Additionally, MOFs could also be combined with other nanoconfined materials to form composite membranes, which could simultaneously utilize the advantages of each component to achieve synergistic higher osmotic power efficiency. Coating functionalized self-assembled UiO-66-NH_2 on a porous anodic aluminum oxide membrane to form heterogeneous sub-nanochannel membranes, Xiao et al. achieved an optimal output power density of 6.76 W m^{-2} and a high Cl^-/SO_4^{2-} selectivity of about 42.2 under a 100-fold NaCl salinity gradient.[93] Furthermore, by introducing imidazole groups on the surface of methylated MOFs, the output power increased to 10.5 W m^{-2} (Fig. 8b). Given the adaptability and versatility of MOFs, it appears that MOFs engineered with responsive molecular functionalities could emerge as prime contenders for inducing ion transfer, thereby harnessing osmotic

forces. Liu et al. successfully prepared light-controllable subnanochannels (SP-MIL-53) encapsulated in spiral polyoxime (SP) using a simple in-situ growth strategy.[94] These highly ordered SP-MIL-53 subnanochannels could effectively regulate ion flux through photo-driven SP isomerization switches, making them intelligent ion-gated controllers capable of achieving a high light response ratio of up to 16.2 in a 10 mM KCl aqueous solution under ultraviolet light irradiation. Moreover, in the open state, these ion-gated subnanochannel membranes exhibited a high power density of 8.3 W m^{-2} under a 50-fold KCl salinity gradient (Fig. 8c). A mixed double-layer MOF-on-MOF membrane was designed to enhance transmembrane conductivity, thereby improving osmotic power generation efficiency. This heterogeneous membrane was constructed by depositing imidazole ester framework-8 (ZIF-8) on a UiO-66-NH_2 membrane containing poly (sodium 4-styrenesulfonate) (PSS).[95] The angstrom-sized pores of the ZIF-8 layer had the ability to enhance ion selectivity through size exclusion, while the PSS interlayer of the UiO-66-NH_2 membrane provided good cation permeability. The synergistic effect of this structure enhanced ion permeability and selectivity simultaneously, achieving an output power of 40.01 W m^{-2} and a current density of 665 A m^{-2} at 3 KΩ resistance under a 500-fold salinity gradient. Additionally, it achieved an efficiency of 9.20 W m^{-2} when treating mixed seawater and river water (Fig. 8d).

The advancement of porous covalent organic framework (COF) materials in osmotic power applications has also witnessed significant strides. Employed as nanofluidic membranes, the highly ordered pore architecture of COFs acts as selective channels, permitting only designated ions to traverse through. This inherent property renders COF nanofluidic membranes particularly well-suited for osmotic power generation.[96] Li

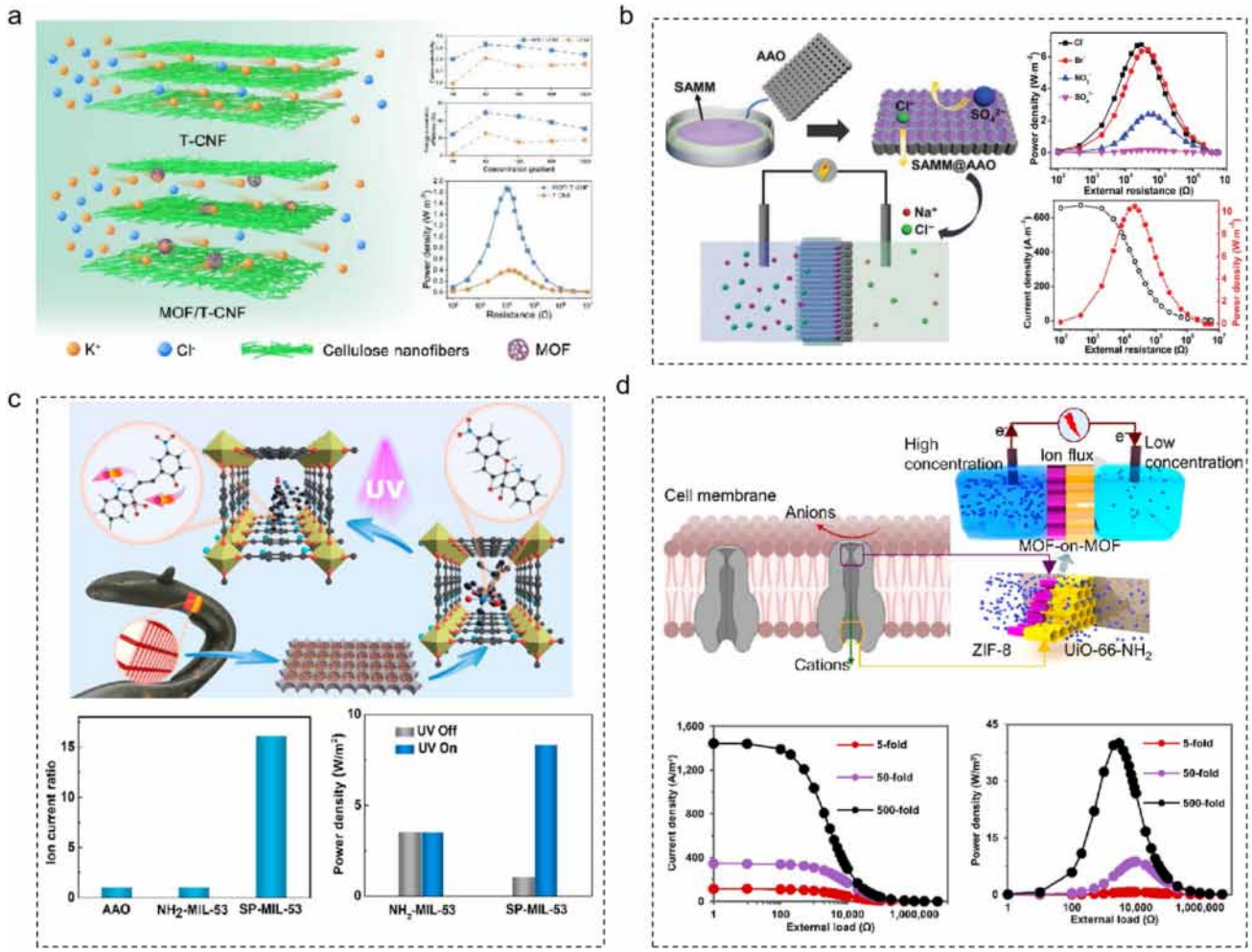

Figure 8. (a) Schematic representation of ion transport through the T-CNF membrane and MOF/T-CNF membrane and the ion selectivity, energy conversion efficiency, and power density. Reproduced with permission from Ref. 92. Copyright © 2023 Elsevier B.V. (b) Schematic illustration of an osmotic power harvesting device and the effect of anion salt types on the current density of the SAMM-2@AAO membrane. Reproduced with permission from Ref. 93. Copyright © 2023 Wiley-VCH GmbH. (c) Schematic representation of the SP-MIL-53 membrane and ionic current ratios and power density. Reproduced with permission from Ref. 94. Copyright © 2022 American Chemical Society. (d) Schematic illustration of the osmotic power generation setup and the current densities and osmotic power densities. Reproduced with permission from Ref. 95. Copyright © 2023 American Chemical Society.

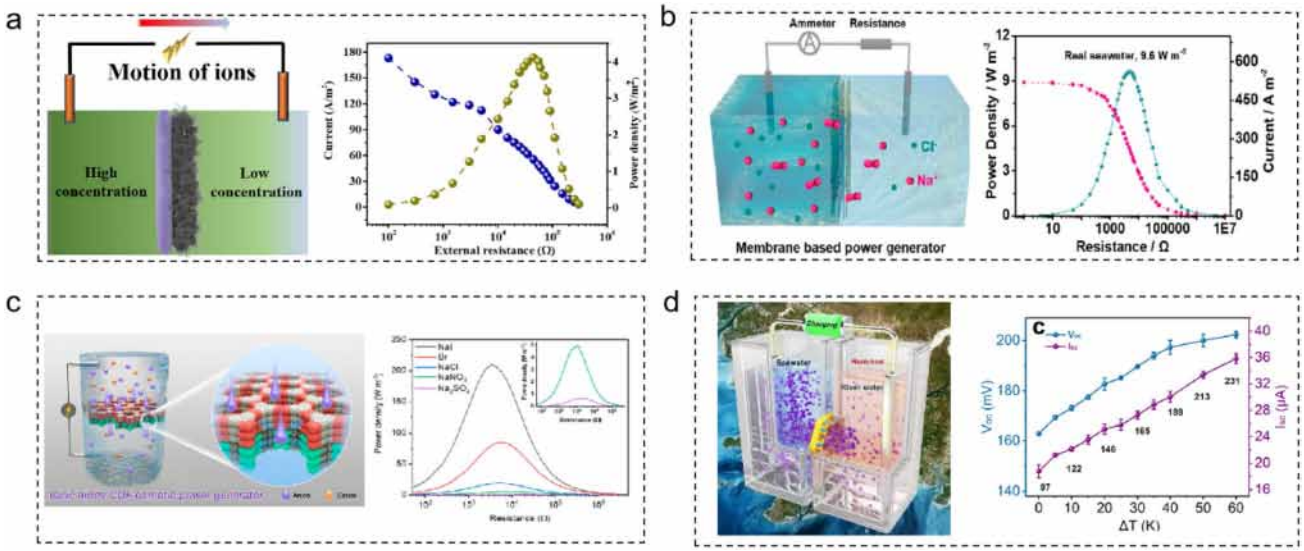

Figure 9. (a) Schematic of osmotic power conversion based on the COF-LZU1@CNT-CNF and the power output. Reproduced with permission from Ref. 97. Copyright © 2022 American Chemical Society. (b) Schematic of the osmotic power conversion process and the output power density of a PyPa-SO_3H/SANF membrane. Reproduced with permission from Ref. 98. Copyright © 2021 American Chemical Society. (c) Salinity-gradient energy harvesting with a TpEB@TpPa-SO_3Na diode membrane and the output power density of various anion salts. Reproduced with permission from Ref. 99. Copyright © 2022 American Chemical Society. (d) Conceptual illustration of the conversion of energies using ionic COF membranes and V_{oc}, I_{sc}, and the corresponding output power density (black numbers) of COF-$(SO_3Na)_1$/PAN in response to the imposed temperature gradients. Reproduced with permission from Ref. 100. Copyright © 2022 Wiley-VCH GmbH.

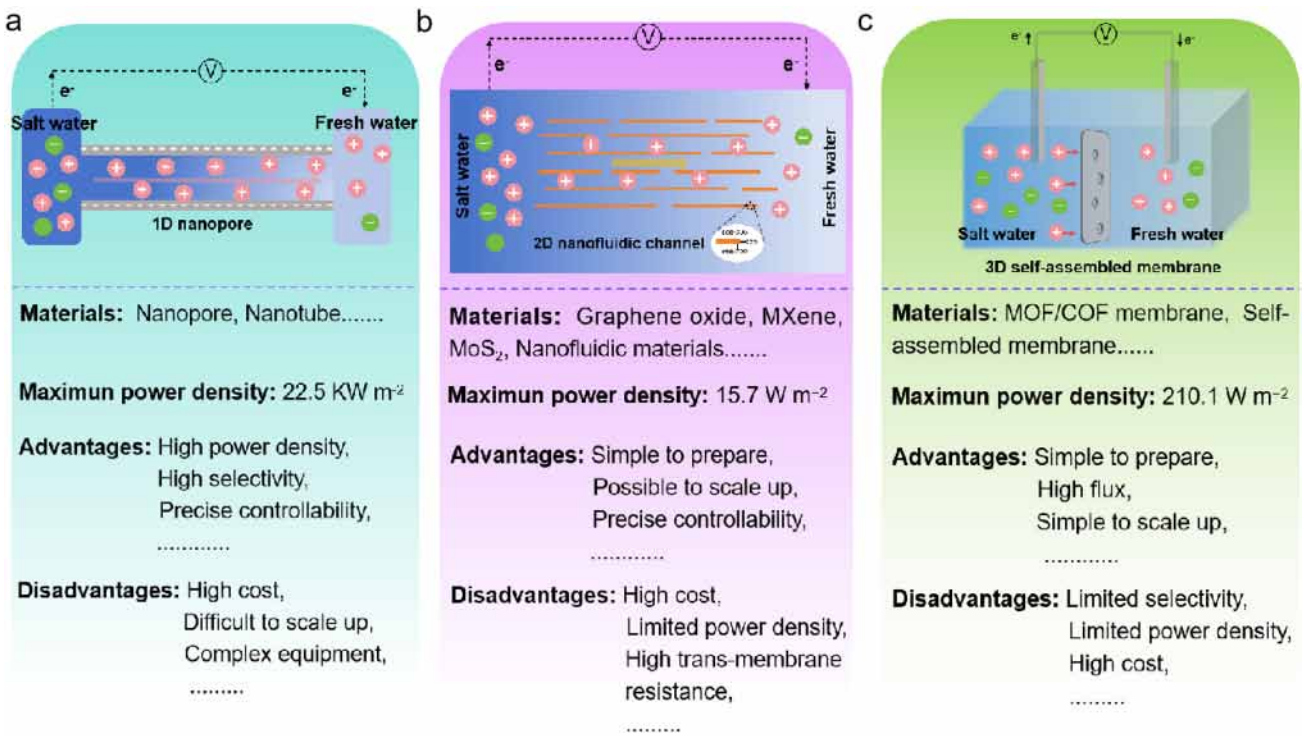

Figure 10. Ion transport under salinity gradient based on (a) 1D nanopore, (b) 2D nanofluidic channel, and (c) 3D self-assembled membrane.

et al. designed a nanofluidic hybrid membrane composed of a highly porous COF, COF-LZU1, and carbon nanotube/cellulose nanofiber (CNT-CNF) membrane.[97] The COF-LZU1 layer, characterized by its meticulously ordered and densely packed pore structure, facilitates rich selectivity for ion transport. Complementarily, the CNT-CNF membrane functions as a robust support layer, furnishing enhanced 3D charged spaces conducive to ion transport. Through this dual-layer configuration, interface ion transport efficiency is significantly enhanced. Through the application of the COF-LZU1@CNT-CNF nanofluidic hybrid membrane for harnessing osmotic power between natural seawater and river water, a notable power density of up to 4.26 W m^{-2} was attained (Fig. 9a). Further optimization of osmotic power generation performance can be achieved through meticulous design of the chemical composition and pore structure of COFs. Coupling sulfonated COFs with anion-grafted aromatic polyamide nanofibers (ANFs) could achieve high-performance osmotic power generation.[98] COFs offered abundant nanofluidic channels conducive to ultra-fast ion migration and achieved high cation permeability through the covalent anchoring of anions. The grafted ANFs enhanced the mechanical strength of the membrane, further improving ion diffusion and rectification. When applied to osmotic power generators, the biomimetic membrane exhibited a power density of 9.6 W m^{-2} (Fig. 9b). Combining asymmetric charges with COF geometrical structures could effectively reduce energy dissipation, further enhancing the energy harvesting performance of osmotic permeability. A COF membrane with clear ion channels, asymmetric geometric shapes, and surface charge polarity was designed, achieving rapid unidirectional ion diffusion and anion selectivity.[99] Density functional theory (DFT) calculations further revealed the differential interactions between anions and COF channels, contributing to superlative I^- transport compared to other anions, achieving output power densities of up to 19.2 W m^{-2} and 210.1 W m^{-2} under 50-fold NaCl and NaI salinity gradients, respectively (Fig. 9c). When incorporating specific thermosensitive organic ligands, synthesized COF membranes exhibited thermally enhanced osmotic power collection phenomena.[100] Transferring the thermosensitive organic ligands triphenylmethane-3,3',5,5'-tetrayltetrakis (benzene-4,1-diyltetrakis (2,1,3-benzoxadiazole)) and diamine compounds (2,5-diaminobenzenesulfonic acid sodium salt and benzene-1,4-diamine) onto polyacrylonitrile (PAN) and growing an active COF layer on the PAN membrane resulted in a composite membrane (COF-$(SO_3Na)_x$/PAN). Adjusting the ratio of diamine compounds during membrane growth controlled the charge density of the resulting membrane. Higher charge density resulted in increased ion selectivity and decreased energy barriers for ion transmembrane transport. Under simulated seawater and river water conditions, the maximum output power density reached 97 W m^{-2}, approximately 20 times that of commercial benchmarks. By applying a temperature gradient, the power density of the optimal membrane-based device reached 231 W m^{-2} in the presence of a 60 K temperature difference (Fig. 9d).

All these works demonstrated that effectively generating energy from salinity gradients through 3D self-assembled membranes was indeed possible and promising. The continuous innovation and optimization of materials such as MOFs and COFs, along with their application in nanofluidic membranes, brought new possibilities to the field of osmotic power generation. The highly ordered porous structures and excellent ion selectivity of these materials make them ideal candidates for efficiently harnessing salinity gradients to produce electricity. From simple nanocomposite membranes to complex COF membrane designs, the potential to achieve high power density outputs under different conditions was evident. Furthermore, the large-scale manufacturing of 3D self-assembled membranes was well-established, with relatively low costs and scalability (Fig. 10c).[101] Furthermore, hierarchical structures, prevalent in natural biological systems like plant roots, facilitate highly efficient mass transfer and exchange with minimal energy consumption. Incorporating these natural principles into 3D self-assembled membranes will enhance osmotic power generation performance through optimized mass transfer and charge regulation. With a deeper understanding of these materials' performance and continuous improvements in the process technology, we can anticipate the emergence of more innovative osmotic power generation technologies in the future, presenting new avenues and opportunities for the renewable energy sector.

Factors affecting ion dynamics

The surface charge and geometric structure of nanoconfined channels profoundly influence osmotic power generation performance.[102] Surface charge dictates ion transport preferences, with various surface chemical modification techniques employed to regulate these properties. Moreover, it directly impacts channel dimensions, ion flow paths, pore structure, and membrane thickness, thereby shaping osmotic power generation. Additionally, asymmetric nanofluidic membranes constructed using nanoconfined materials with different charge types or geometric properties may yield unconventional osmotic performance. Beyond surface charge and geometric structure, external stimuli such as pH, solution temperature, light, thermal gradients, electrical fields, magnetic fields, and pressure gradients also influence osmotic power generation. This section systematically discusses the intricate relationship between these factors and osmotic power generation, drawing from recent experimental and theoretical insights.

Surface charge

In nanofluidics, the presence of the EDL underscores the paramount importance of surface charge regulation. The charge polarity exhibited on the channel surface directly determines its ion selectivity. Therefore, by adjusting the surface charge, the ion transport characteristics of nanoconfined channels could be effectively controlled. In the preparation process of nanoconfined materials, specific ionizable functional groups could be introduced onto their surfaces. These functional groups can partially ionize in water, leading to the charging of channel surfaces and the formation of nanoconfined channels with tailored

surface charge properties. It has been observed that introducing vacancies in nanoconfined materials can further augment the surface charge of these channels.

Furthermore, the surface charge density significantly influences osmotic power conversion by regulating the formation and attributes of the EDL, which, in turn, dictates interactions between nanoconfined membrane or material surfaces and solution ions. This influence governs osmotic pressure and fluid movement, resulting in heightened membrane selectivity, optimized ion flux, and enhanced energy conversion efficiency within osmotic power systems. However, excessively high surface charge density may exacerbate electrostatic attraction between the membrane surface and solution ions, potentially leading to ion accumulation or deposition on the nanoconfined membrane surface. This phenomenon can increase membrane resistance and diminish ion flux. For example, Hsu et al. reported on a single funnel-shaped nanochannel (FSN), which defied the previous relationship between surface charge density and permeability performance.[103] The permeability performance decreased with increasing surface charge density due to the significant increase in surface charge density amplifying the ion concentration polarization effect (ICP), thereby weakening the effective salinity ratio across the entire channel and reducing osmotic power conversion performance.

In addition, composite nanoconfined materials endowed with asymmetric charge properties, formed by combining materials with different charge polarities, exhibited significant performance advantages. An asymmetric ion exchange membrane based on MMT and its blend with PAA and PEI (MAME) demonstrated a unique asymmetric composite construction and different surface charge properties.[104] This asymmetrical surface nature, in conjunction with Janus channel dimensions, facilitated precise control over ion transport within nanochannels, thereby evincing a pronounced nanofluidic diode effect.

Geometric Structure

Optimizing membrane structure design is paramount for enhancing osmotic power conversion efficiency. The key challenge lies in precisely tuning the membrane structure to facilitate rapid passage of counter-ions while effectively blocking co-ions to achieve high-selectivity. It is widely recognized that reducing channel size can enhance ion selectivity, thereby generating a higher osmotic voltage. However, larger channel diameters, while potentially reducing ion selectivity, offer advantages in increasing ion flux, thereby enabling more efficient osmotic power harvesting. Therefore, selecting the optimal nanoconfined channel size is crucial for maximizing energy conversion efficiency, necessitating a delicate balance between ion selectivity and permeability.[91] Additionally, the efficiency of energy conversion was also influenced by the length of the ion transport path. Broadly speaking, as the length of the ion transport path increased, both the diffusion current density and power density decreased due to the heightened resistance encountered by migrating ions, a phenomenon that aligned with the classic Ohmic response. For instance, Sun et al. synthesized bipolar membranes using non-solvent-induced phase separation (NIPS) and spin coating (SC) techniques employing polymers with identical poly (ether sulfone) backbones but opposing charges.[105] They noted a decline in power density from 4.5 to 2.1 W m^{-2} as the length of the ion transport path increased, attributed to elevated internal resistance hindering ion transport and diminishing energy density (Fig. 11a). Chen et al. engineered a nanoscale silk fibroin (SF) membrane for osmotic energy harvesting, unveiling an unexpected correlation between osmotic power conversion performance and the thickness of the SF membrane.[106] When the membrane thickness was at 100 nm, the current density reached its maximum value of 225 A m^{-2}, and the power density peaked at 4.06 W m^{-2} between seawater and river water. This was due to the ICP effect being more pronounced in thinner nanoconfined channels where local concentration deviations were more evident, leading to accumulated ions permeating the channel and causing an increase in ion concentration on the low concentration side, effectively reducing the salinity gradient. In contrast, thicker nanoconfined channels exhibited a diminished ICP effect, which augmented the output power density.

In addition to the dimensions of the nanoconfined channels, the geometrical shape of the nanoconfined channels played a pivotal role in modulating the ion transportation dynamics. Ramírez et al. conducted simulations on conical, trumpet-like, and bullet-like nanopores, revealing that the morphology of the nanopores played a critical role in determining the transmembrane current and ion selectivity of the device.[107] Compared to conical and trumpet-like nanopores, bullet-like nanopores could offer a better trade between ion selectivity and ion permeability. Since single conic tracks were basic components of nanoporous membranes, understanding and controlling their performance was also essential in osmotic power applications (Fig. 11b). Ion-track-etched polyethylene terephthalate (PET) substrates were used to create bullet-like nanopores, which undergo significant constriction near the exit to yield a minute aperture.[108] This design achieved an output power density of up to 80 picowatts under optimized conditions, significantly surpassing the performance of unmodified PET channels. The Poisson-Nernst-Planck (PNP) model further revealed that the high power density of this channel was due to the geometric shape of the bullet-shaped nanopore, which, compared to other shapes, had a larger channel volume and a greater product of current and reversal potential, thus favoring power generation. Lu et al. used a nanoconfined assembly strategy to asymmetrically grow MOF crystals in bullet-like PET NCs, producing PET/MIL-53-COOH NCs, which achieved unidirectional ultra-fast reverse transport of alkaline metal ions and protons.[109] Under a tenfold HCl salinity gradient, a super high proton output power density of 4509 W m^{-2} was achieved.

External factors

To enhance osmotic power efficiency, researchers have explored integrating additional external stimuli, such as pH,

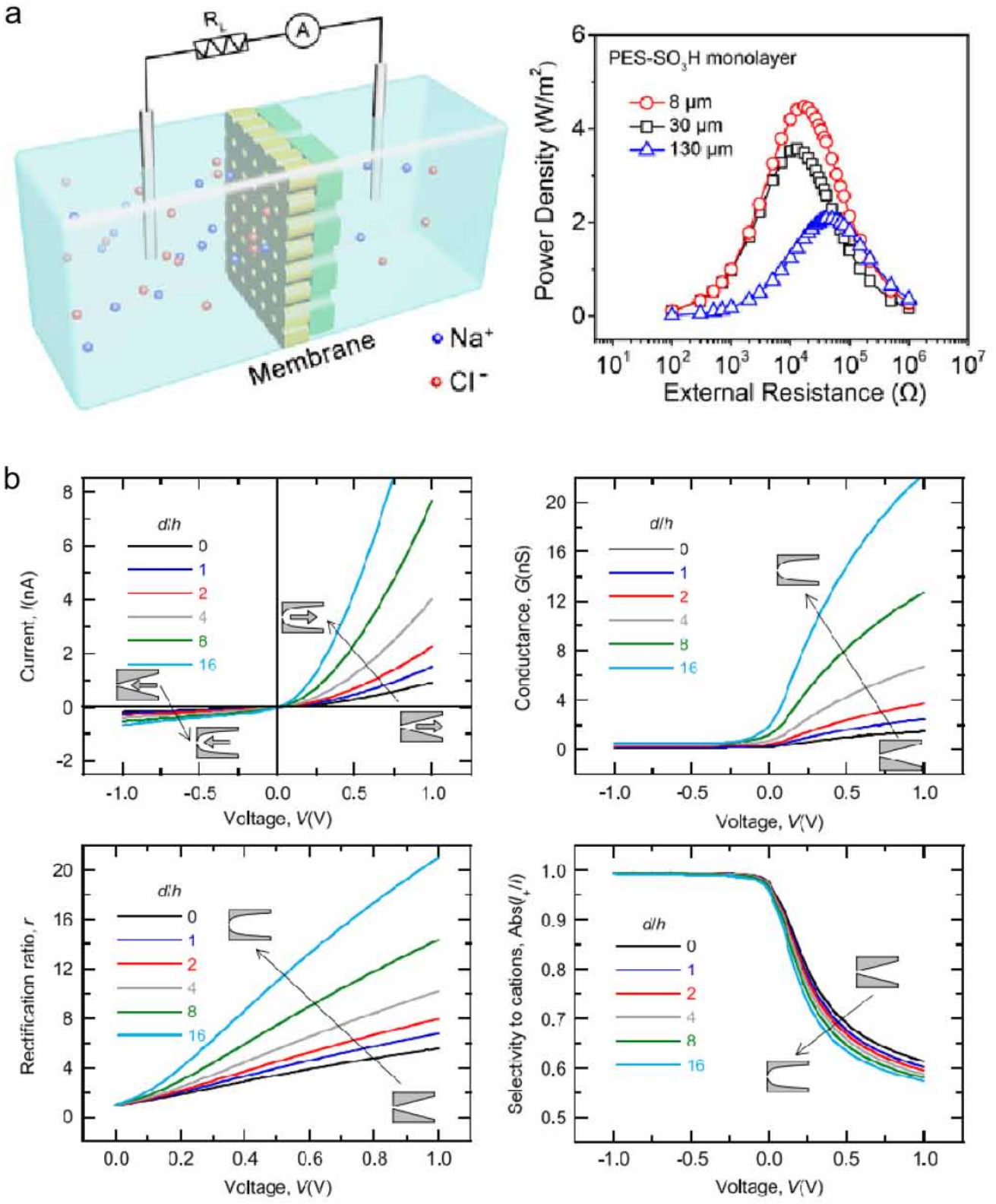

Figure 11. (a) A device for testing the electrochemical properties of the bipolar membrane and output power densities of different thicknesses under a 50-fold salinity gradient. Reproduced with permission from Ref. 105. Copyright © 2020 Wiley-VCH GmbH. (b) The electrochemical properties of conical, trumpet-like, and bullet-like nanopores. Reproduced with permission from Ref. 107. Copyright © 2008 IOP Publishing Ltd.

temperature, light, thermal gradients, electrical fields, magnetic fields, and pressure gradients. These external factors provide supplementary driving forces that synergize with salinity gradients, leading to significant improvements in energy conversion efficiency.[110–112]

The pH value significantly impacts the performance of osmotic membranes by directly affecting the charge state and structural stability of the membrane materials. Variations in pH conditions alter the charged characteristics of the membrane surface, influencing its ability to attract or repel ions and thereby affecting ion transport and overall membrane efficiency. For example, the $Mo_2TiC_2T_x$ MXene membrane achieved a power density of 13.1 W m^{-2} in an alkaline (pH = 9) KCl solution, owing to the increased surface negative charge density in the alkaline solution (Fig. 12a).[113] Increasing the temperature of the solution could also enhance osmotic power conversion performance, as temperature affects the properties of the solution and the solid–liquid interface. Increasing temperature lowers solution viscosity and heightens ion diffusion rates, expediting ion transport and boosting ion flux. Additionally, higher temperatures can enhance surface charge density and ion selectivity by altering interface chemical reactions, thereby improving osmotic power conversion performance. In the case of the PNIPAM-g-sCC membrane, when the temperature increased from 25 to 50 °C, the short-circuit current (I_{sc}) was 10.25 μA, approximately fourfold that at 25 °C, the open-circuit voltage (V_{oc}) increased from 107 to 125 mV, and the power density increased from 6.75 to 27 W m^{-2} (Fig. 12b).[114]

In recent years, light has emerged as a promising driving force for active ion transport based on photoelectric and photothermal mechanisms. Notably, GO generated significant ionic currents under illumination.[115,116] Additionally, light energy could induce responsive ion transport in artificial nanoconfined channels, making the combination of osmotic power and light energy more effective in harnessing energy, thus enhancing power output performance.[117] For instance, Wen et al. utilized a WS_2 composite membrane for osmotic power conversion.[118] When subjected to

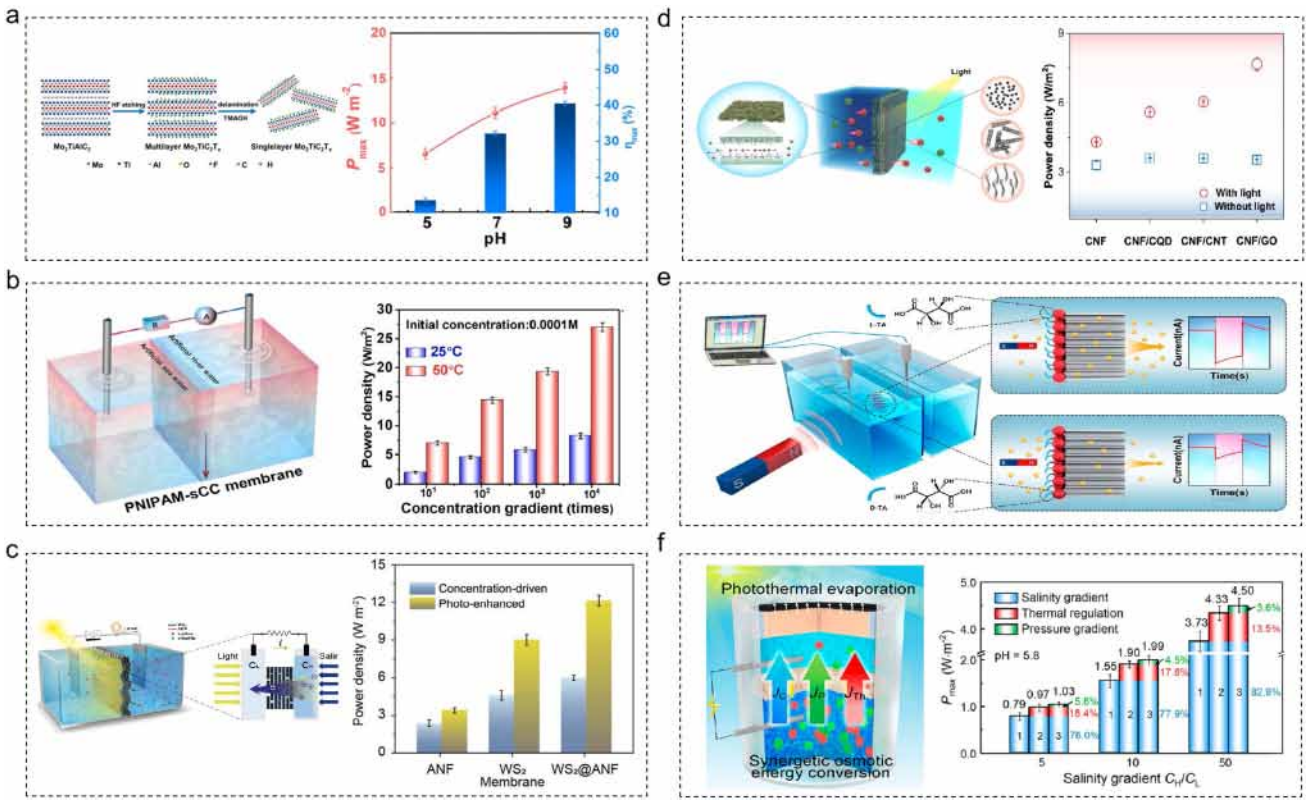

Figure 12. (a) The mechanism schematic of the $Mo_2TiC_2T_x$ MXene nanoconfined channels and the power density and energy conversion efficiency at different pH KCl solutions. Reproduced with permission from Ref. 113. Copyright © 2022 IOP Publishing Ltd. (b) Schematic illustration of the PNIP AM-sCC membrane and the power density with the salinity gradient at temperatures of 25 ℃ and 50 ℃. Reproduced with permission from Ref. 114. Copyright © 2018 The Royal Society of Chemistry. (c) Schematic of the solar-driven osmotic power conversion system platform and the output power comparison of pristine WS_2 and ANF membranes as well as the WS_2@ANF composite membranes before and after light irradiation. Reproduced with permission from Ref. 118. Copyright © 2023 Wiley-VCH GmbH. (d) Schematic of the combination photothermal-enhanced osmotic power conversion by constructing a CNF/LDCM nanofluidic membrane and the power density of the CNF/LDCM membranes under light irradiation. Reproduced with permission from Ref. 119. Copyright © 2022 Wiley-VCH GmbH. (e) Diagram depicting ion transport dependent on chirality with magnetic gating. Reproduced with permission from Ref. 120. Copyright © 2022, American Chemical Society. (f) An illustrative depiction of GO-based nanochannels for osmotic power conversion and the synergy of thermal regulation and pressure gradient on power density. Reproduced with permission from Ref. 121. Copyright © 2024, American Chemical Society.

both light and a 50-fold NaCl salinity gradient, the power density increased from 6.01 to 12.43 W m^{-2} (Fig. 12c). The photothermal response of nanoconfined materials was another effective method for enhancing osmotic power conversion. For example, Luo et al. developed a cellulose nanofiber (CNF) membrane incorporating ultrathin low-dimensional carbon materials (LDCM) to enhance osmotic power conversion through photothermal effects.[119] When subjected to light irradiation and a 50-fold salinity gradient, the output power density of the osmotic generator rose from 3.55 to 7.67 W m^{-2} (Fig. 12d). Additionally, magnetic fields have also been utilized to control ion transport in nanoconfined spaces, leading to the generation of ionic currents. The Lorentz force acting on charged particles under a magnetic field can deflect their paths, enabling precise control over ion transport paths and speeds by adjusting the field's strength and direction. For instance, a chiral magnetic iron oxide nanofilm with nanoconfined channels modified with L-tartaric acid (TA) was prepared.[120] Under the influence of a magnetic field, an immediate ionic current of 8.2 nA was generated. Upon continuous action for 30s, the current gradually stabilized at 6.8 nA. When the external magnetic field was perpendicular to the nanoconfined channels, the ionic current rapidly decayed, eventually reaching an inverse ionic current of approximately 1.63 nA before returning to zero. Post-magnetic field application, ion permeability of nanoconfined channels increased, attributed to the dehydration of ions by the magnetic system, thereby reducing the energy loss required for ion transport through the membrane barrier (Fig. 12e).

Furthermore, the combination of pressure gradients and temperature gradients, in conjunction with additional surface charge density, could enhance the charge repulsion or attraction effects on the nanoconfined channel surface, thereby regulating the selective transfer of ions or molecules through the membrane. This effect could reduce osmotic resistance and increase ion permeability while possibly reducing membrane fouling, thereby enhancing the membrane's lifespan and the system's overall performance. Thus, utilizing the synergistic effects of surface charge with temperature and pressure gradients optimizes the osmotic process and enhances osmotic efficiency. For instance, in GO-based nanochannels, the combined influence of salinity gradients and pressure gradients under thermoregulation resulted in a significant enhancement in osmotic power generation performance (Fig. 12f).[121]

Conclusion and perspectives

Nanoconfined materials of different dimensions (1D, 2D, and 3D) were widely used to construct nanoconfined channel membranes for osmotic power harvesting. 1D nanopores exhibit high ion selectivity, ion permeability, and output power density (22.5 kW m^{-2}) due to precise control over their geometric structure and chemical properties. Fabricated by the ion-track-etched technique, 1D nanopore materials provide the theoretical framework for studying the principles of salinity gradient energy conversion. However, their practical application in osmotic energy is constrained by polarization, high fabrication costs, and challenges in scaling up. 2D layered membranes, such as GO and MXene, possess a large specific surface area and are easy to be modified, allowing regulation of ion selectivity in nanoconfined channels and enabling higher ion flux and scalability. Typically prepared by the vacuum filtration method, these membranes are straightforward to fabricate and modify, but the trade-off between ion selectivity and ion permeability remains a challenge. Moreover, 2D layered membranes have high transmembrane resistance, limiting their output power density (15.7 W m^{-2}). Through the layer-by-layer self-assembly method, 3D self-assembled membranes, distinguished by their cost-effective fabrication, scalability, and tunable surfaces, can attain a higher output power density of 210.1 W m^{-2} improved efficient mass transfer and charge regulation. Moreover, their robust structural stability enhances scalability, thereby increasing their potential for practical applications in osmotic power generation.

The diversity of nanoconfined materials enabled them to exhibit different performance characteristics, which could be further optimized through physicochemical modifications, enhancing osmotic power conversion efficiency. Moreover, external environmental factors like pH, temperature, light, thermal gradients, electricity, and magnetism can also influence osmotic power generation performance. Therefore, nanoporous membrane channels might hold tremendous potential for addressing the challenges of achieving efficient osmotic power generation.

Ion transport behaviors (ion selectivity and ion permeability) are pivotal in osmotic power generation, directly influencing energy conversion. Within nanoconfined channels, these behaviors, including ion diffusion, migration, and selective permeation, profoundly impact membrane permeability and power conversion efficiency. Firstly, the ion diffusion rate dictates ion flux and power density output. Secondly, ion migration behavior governs channel selectivity. Additionally, ion interactions during permeation affect power density output. Membrane thickness is critical for optimal power generation, requiring a balance between selectivity, permeability, and scalability challenges. Thicker membranes typically possess higher mechanical stability and ion selectivity, which are crucial for maintaining membrane structural stability and reliable separation processes. However, thicker membranes might also result in lower ion permeability, limiting the enhancement of energy conversion efficiency. Conversely, thinner membranes might enhance ion permeability but might sacrifice some degree of ion selectivity and mechanical strength, thereby affecting system stability and long-term operational capacity. Therefore, in designing and optimizing osmotic power conversion systems, a balance point in membrane thickness must be found to simultaneously consider ion selectivity, ion permeability, membrane structural stability and mechanical performance. Additionally, with the development of osmotic power conversion technology, membrane size scaling was also a significant concern, as it directly affected the practical application and economic feasibility of the system. Thus, comprehensive consideration of factors such as ion selectivity, ion permeability, and scalability were essential to achieving efficient and stable osmotic power conversion performance.

Nanoconfined materials are extensively utilized in crafting ion-selective membranes, with properties like photothermal conversion showing promise in enhancing osmotic power harvesting. However, the numerous unique properties of nanoconfined materials had not yet been fully explored, particularly in addressing the trade-off between ion selectivity and permeability. In osmotic power conversion, mass transfer within nanoconfined materials influences diffusion rates, while electrostatic interactions affect charge distribution and surface adsorption. This synergistic effect between mass transfer and electrostatic interactions plays a pivotal role in balancing ion selectivity and permeability. The presence of hierarchical structures, commonly found in natural organisms to facilitate effective mass transportation, along with the distinctive dynamic behaviors of ions within nanoconfined systems, present opportunities for efficient unipolar ion transport. Modifying membrane microstructure, including pore size and shape, influences mass transport dynamics such as ion diffusion rates and migration. Additionally, specific charged functional groups within nanoconfined spaces dictate ion dynamics, affecting ion adsorption and repulsion behaviors. Synergizing enhanced mass transport with ion dynamics in multi-hierarchical structured materials with tailored charge might resolve the selectivity-permeability balance with scalability possibility, hold promise for ushering in a new era of highly efficient osmotic power generation.

Author contributions

Lixue Yang: Conceptualization, Writing-original draft; Shaoxin Li: Editing; Han Qian: Conceptualization; Zhe Wang: Supervision; Di Wei: Conceptualization, Writing-reviewing and editing, Supervision, Funding acquisition; Zhong Lin Wang: Conceptualization, Supervision, Funding acquisition.

Funding

This work was supported by the Beijing Natural Science Foundation (Grant No. IS23040).

Data availability

No applicable.

Code availability

No code was written or used.

Declarations

Conflict of interest

The authors declare no potential conflicts.

Ethical approval

We follow the ethical code of conduct of the MRS Energy and Sustainability.

Consent to participate

All authors consent to participate in this review.

Consent for publication

All authors give their consent for publication in the journal MRS Energy and Sustainability.

REFERENCES

1. Z. Liu, Z. Deng, G. He, H. Wang, X. Zhang, J. Lin, Y. Qi, X. Liang, Challenges and opportunities for carbon neutrality in China. Nat. Rev. Earth Environ. **3**(2), 141–155 (2022). https://doi.org/10.1038/s43017-021-00244-x
2. D.J. Davidson, Exnovating for a renewable energy transition. Nat. Energy **4**(4), 254–256 (2019). https://doi.org/10.1038/s41560-019-0369-3
3. F. Hashemifar, A. Esfandiar, Oppositely charged MXene fibers as a highly efficient osmotic power generator from sea and river water. J. Mater. Chem. A **10**(46), 24915–24926 (2022). https://doi.org/10.1039/D2TA06557F
4. B.E. Logan, M. Elimelech, Membrane-based processes for sustainable power generation using water. Nature **488**(7411), 313–319 (2012). https://doi.org/10.1038/nature11477
5. J. Seo, K.H. Jensen, W. Kim, Concentration-responsive soft valve for osmotic flow control. ACS Appl. Mater. Interfaces **13**(38), 46015–46021 (2021). https://doi.org/10.1021/acsami.1c14282
6. M. Zhang, N. Sheng, Q. Song, H. Zhang, S. Chen, H. Wang, K. Zhang, Enhanced selective ion transport by assembling nanofibers to membrane pairs with channel-like nanopores for osmotic energy harvesting. Nano Energy **103**, 107786 (2022). https://doi.org/10.1016/j.nanoen.2022.107786
7. L. Cao, I.C. Chen, C. Chen, D.B. Shinde, X. Liu, Z. Li, Z. Zhou, Y. Zhang, Y. Han, Z. Lai, Giant osmotic energy conversion through vertical-aligned ion-permselective nanochannels in covalent organic framework membranes. J. Am. Chem. Soc. **144**(27), 12400–12409 (2022). https://doi.org/10.1021/jacs.2c04223
8. H. Qian, D. Wei, Z. Wang, Bionic iontronics based on nano-confined structures. Nano Res. **16**(9), 11718–11730 (2023). https://doi.org/10.1007/s12274-023-5705-z
9. M. Tsutsui, K. Yokota, I.W. Leong, Y. He, T. Kawai, Sparse multi-nanopore osmotic power generators. Cell Rep. Phys. Sci. **3**(10), 101065 (2022). https://doi.org/10.1016/j.xcrp.2022.101065
10. A.R. Koltonow, J. Huang, Two-dimensional nanofluidics. Science **351**(6280), 1395–1396 (2016). https://doi.org/10.1126/science.aaf5289
11. K. Xiao, L. Jiang, M. Antonietti, Ion transport in nanofluidic devices for energy harvesting. Joule **3**(10), 2364–2380 (2019). https://doi.org/10.1016/j.joule.2019.09.005
12. K. Zhan, Z. Li, J. Chen, Y. Hou, J. Zhang, R. Sun, Z. Bu, L. Wang, M. Wang, X. Chen, X. Hou, Tannic acid modified single nanopore with multivalent metal ions recognition and ultra-trace level detection. Nano Today **33**, 100868 (2020). https://doi.org/10.1016/j.nantod.2020.100868
13. M. Tsutsui, W.-L. Hsu, D. Garoli, I.W. Leong, K. Yokota, H. Daiguji, T. Kawai, Gate-all-around nanopore osmotic power generators. ACS Nano **18**(23), 15046–15054 (2024). https://doi.org/10.1021/acsnano.4c01989
14. L. Yang, F. Yang, X. Liu, K. Li, Y. Zhou, Y. Wang, T. Yu, M. Zhong, X. Xu, L. Zhang, W. Shen, D. Wei, A moisture-enabled fully printable power source inspired by electric eels. PNAS **118**(16), e2023164118 (2021). https://doi.org/10.1073/pnas.2023164118

15. F. Zhang, J. Yu, Y. Si, B. Ding, Meta-aerogel ion motor for nanofluid osmotic energy harvesting. Adv. Mater. **35**(38), 2302511 (2023). https://doi.org/10.1002/adma.202302511
16. P. Peng, H. Qian, J. Liu, Z. Wang, D. Wei, Bioinspired ionic control for energy and information flow. Int. J. Smart Nano Mat. **15**(1), 198–221 (2024). https://doi.org/10.1080/19475411.2024.2305393
17. A. Rozov, Y. Zakharova, A. Vazetdinova, F. Valiullina-Rakhmatullina, The role of polyamine-dependent facilitation of calcium permeable AMPARs in short-term synaptic enhancement. Front. Cell. Neurosci. (2018). https://doi.org/10.3389/fncel.2018.00345
18. T. Xiao, B. Lu, Z. Liu, Q. Zhang, J. Zhai, X. Diao, Action-potential-inspired osmotic power generation nanochannels. J. Membrane Sci. **642**, 119999 (2022). https://doi.org/10.1016/j.memsci.2021.119999
19. E. Badoer, C.-W. Ng, R.D. Matteo, Glutamatergic input in the PVN is important in renal nerve response to elevations in osmolality. Am. J. Physiol. Renal **285**(4), 640–650 (2003). https://doi.org/10.1152/ajprenal.00372.2002
20. X. Zheng, G. Shen, C. Wang, Y. Li, D. Dunphy, T. Hasan, C.J. Brinker, B.-L. Su, Bio-inspired Murray materials for mass transfer and activity. Nat. Commun. **8**(1), 14921 (2017). https://doi.org/10.1038/ncomms14921
21. S. Li, J. Wang, Y. Lv, Z. Cui, L. Wang, Nanomaterials-based nanochannel membrane for osmotic energy harvesting. Adv. Funct. Mater. **34**(4), 2308176 (2024). https://doi.org/10.1002/adfm.202308176
22. Y. Jiao, C. Yang, W. Zhang, Q. Wang, C. Zhao, A review on direct osmotic power generation: mechanism and membranes. Renew. Sust. Energ. Rev. **191**, 114078 (2024). https://doi.org/10.1016/j.rser.2023.114078
23. J. Wang, Y. Zhou, L. Jiang, Bioinspired three-dimensional nanoporous membranes for salinity-gradient energy harvesting. Acc. Mater. Res. **4**(1), 86–100 (2023). https://doi.org/10.1021/accountsmr.2c00210
24. Z. Zhang, L. Wen, L. Jiang, Nanofluidics for osmotic energy conversion. Nat. Rev. Mater. **6**(7), 622–639 (2021). https://doi.org/10.1038/s41578-021-00300-4
25. D. Lei, Z. Zhang, L. Jiang, Bioinspired 2D nanofluidic membranes for energy applications. Chem. Soc. Rev. **53**(5), 2300–2325 (2024). https://doi.org/10.1039/D3CS00382E
26. H. Zhang, X. Li, J. Hou, L. Jiang, H. Wang, Angstrom-scale ion channels towards single-ion selectivity. Chem. Soc. Rev. **51**(6), 2224–2254 (2022). https://doi.org/10.1039/D1CS00582K
27. X. Tong, S. Liu, J. Crittenden, Y. Chen, Nanofluidic membranes to address the challenges of salinity gradient power harvesting. ACS Nano **15**(4), 5838–5860 (2021). https://doi.org/10.1021/acsnano.0c09513
28. W.-X. Pan, L. Chen, W.-Y. Li, Q. Ma, H. Xiang, N. Ma, X. Wang, Y. Jiang, F. Xia, M. Zhu, Scalable fabrication of ionic-conductive covalent organic framework fibers for capturing of sustainable osmotic energy. Adv. Mater. (2024). https://doi.org/10.1002/adma.202401772
29. Y.-C. Liu, L.-H. Yeh, M.-J. Zheng, K.C.-W. Wu, Highly selective and high-performance osmotic power generators in subnanochannel membranes enabled by metal-organic frameworks. Sci. Adv. **7**(10), eabe9924 (2021). https://doi.org/10.1126/sciadv.abe9924
30. Y. Ma, L.-H. Yeh, C.-Y. Lin, L. Mei, S. Qian, pH-regulated ionic conductance in a nanochannel with overlapped electric double layers. Anal. Chem. **87**(8), 4508–4514 (2015). https://doi.org/10.1021/acs.analchem.5b00536
31. D. Wei, Writable electrochemical energy source based on graphene oxide. Sci. Rep. **5**(1), 15173 (2015). https://doi.org/10.1038/srep15173
32. H. Li, F. Xiao, G. Hong, J. Su, N. Li, L. Cao, Q. Wen, W. Guo, On the role of heterogeneous nanopore junction in osmotic power generation. Chinese J. Chem. **37**(5), 469–473 (2019). https://doi.org/10.1002/cjoc.201900042
33. S. Zhou, L. Xie, L. Zhang, L. Wen, J. Tang, J. Zeng, T. Liu, D. Peng, M. Yan, B. Qiu, Q. Liang, K. Liang, L. Jiang, B. Kong, Interfacial super-assembly of ordered mesoporous silica–alumina heterostructure membranes with pH-sensitive properties for osmotic energy harvesting. ACS Appl. Mater. Interfaces **13**(7), 8782–8793 (2021). https://doi.org/10.1021/acsami.0c21661
34. J. Wang, L. Wang, N. Shao, M. He, P. Shang, Z. Cui, S. Liu, N. Jiang, X. Wang, L. Wang, Heterogeneous Two-dimensional lamellar $Ti_3C_2T_x$ membrane for osmotic power harvesting. Chem. Eng. J. **452**, 139531 (2023). https://doi.org/10.1016/j.cej.2022.139531
35. B. Yuan, H. Sun, S. Zhao, H. Yang, P. Wang, P. Li, H. Sun, Q. Jason Niu, Semi-aromatic polyamide nanofiltration membranes with tuned surface charge and pore size distribution designed for the efficient removal of Ca^{2+} and Mg^{2+}. Sep. Purif. Technol. **220**, 162–175 (2019). https://doi.org/10.1016/j.seppur.2019.03.063
36. X. Zhu, Y. Zhou, J. Hao, B. Bao, X. Bian, X. Jiang, J. Pang, H. Zhang, Z. Jiang, L. Jiang, A charge-density-tunable three/two-dimensional polymer/graphene oxide heterogeneous nanoporous membrane for ion transport. ACS Nano **11**(11), 10816–10824 (2017). https://doi.org/10.1021/acsnano.7b03576
37. X. Hong, X.-J. Huang, Q.-L. Gao, H.-M. Wu, Y.-Z. Guo, F. Huang, F. Fang, H.-T. Huang, D.-J. Chen, Microstructure–performance relationships of hollow-fiber membranes with highly efficient separation of oil-in-water emulsions. J. Appl. Polym. Sci. **136**(23), 47615 (2019). https://doi.org/10.1002/app.47615
38. Y. Tao, W. Liu, Y. Ren, Y. Hu, G. Li, G. Ma, Q. Wu, On Developing field-effect-tunable nanofluidic ion diodes with bipolar, induced-charge electrokinetics. Micromachines **9**(4), 179 (2018). https://doi.org/10.3390/mi9040179
39. K. Xiao, G. Xie, Z. Zhang, X.-Y. Kong, Q. Liu, P. Li, L. Wen, L. Jiang, Enhanced stability and controllability of an ionic diode based on funnel-shaped nanochannels with an extended critical region. Adv. Mater. **28**(17), 3345–3350 (2016). https://doi.org/10.1002/adma.201505842
40. W.-H. Zhang, M.-J. Yin, Q. Zhao, C.-G. Jin, N. Wang, S. Ji, C.L. Ritt, M. Elimelech, Q.-F. An, Graphene oxide membranes with stable porous structure for ultrafast water transport. Nat. Nanotechnol. **16**(3), 337–343 (2021). https://doi.org/10.1038/s41565-020-00833-9
41. J. Wan, L. Huang, J. Wu, L. Xiong, Z. Hu, H. Yu, T. Li, J. Zhou, Microwave combustion for rapidly synthesizing pore-size-controllable porous graphene. Adv. Funct. Mater. **28**(22), 1800382 (2018). https://doi.org/10.1002/adfm.201800382
42. R. Sharma, M. Geranpayehvaghei, F. Ejeian, A. Razmjou, M. Asadnia, Recent advances in polymeric nanostructured ion selective membranes for biomedical applications. Talanta **235**, 122815 (2021). https://doi.org/10.1016/j.talanta.2021.122815
43. W. Li, W. Wang, Y. Zhang, Y. Yan, C. Dai, J. Zhang, Gated water transport through graphene nanochannels: from ionic coulomb blockade to electroosmotic pump. J. Phys. Chem. C **121**(32), 17523–17529 (2017). https://doi.org/10.1021/acs.jpcc.7b05374
44. J.R. Whicher, R. MacKinnon, Structure of the voltage-gated K^+ channel Eag1 reveals an alternative voltage sensing mechanism. Science **353**(6300), 664–669 (2016). https://doi.org/10.1126/science.aaf8070
45. I.K. Kaufman, P.V.E. McClintock, R.S. Eisenberg, Coulomb blockade model of permeation and selectivity in biological ion channels. New J. Phys. **17**(8), 083021 (2015). https://doi.org/10.1088/1367-2630/17/8/083021
46. T. Huang, X. Kan, J. Fan, H. Gao, L. Yu, L. Zhang, J. Xia, J. Gao, X. Liu, K. Sui, L. Jiang, Two-dimensional sodium channels with high selectivity and conductivity for osmotic power generation from wastewater. ACS Nano **17**(17), 17245–17253 (2023). https://doi.org/10.1021/acsnano.3c05149

47. W. Guo, L. Cao, J. Xia, F.-Q. Nie, W. Ma, J. Xue, Y. Song, D. Zhu, Y. Wang, L. Jiang, Energy harvesting with single-ion-selective nanopores: a concentration-gradient-driven nanofluidic power source. Adv. Funct. Mater. **20**(8), 1339–1344 (2010). https://doi.org/10.1002/adfm.200902312
48. A. Siria, P. Poncharal, A.-L. Biance, R. Fulcrand, X. Blase, S.T. Purcell, L. Bocquet, Giant osmotic energy conversion measured in a single transmembrane boron nitride nanotube. Nature **494**(7438), 455–458 (2013). https://doi.org/10.1038/nature11876
49. J. Feng, M. Graf, K. Liu, D. Ovchinnikov, D. Dumcenco, M. Heiranian, V. Nandigana, N.R. Aluru, A. Kis, A. Radenovic, Single-layer MoS_2 nanopores as nanopower generators. Nature **536**(7615), 197–200 (2016). https://doi.org/10.1038/nature18593
50. M. Majumder, N. Chopra, R. Andrews, B.J. Hinds, Enhanced flow in carbon nanotubes. Nature **438**(7064), 44–44 (2005). https://doi.org/10.1038/438044a
51. G. Cui, Z. Xu, H. Li, S. Zhang, L. Xu, A. Siria, M. Ma, Enhanced osmotic transport in individual double-walled carbon nanotube. Nat. Commun. **14**(1), 2295 (2023). https://doi.org/10.1038/s41467-023-37970-3
52. Z. Liu, T. Chen, G. Liu, Effect of the dielectric membrane channel on salinity gradient energy conversion. Desalination **574**, 117287 (2024). https://doi.org/10.1016/j.desal.2023.117287
53. S. Shirahama, S. Zhang, M. Aiba, H. Inoue, M. Hada, Y. Hayashi, K. Hata, S. Tsuruoka, H. Matsumoto, Temperature dependence of pressure-driven water permeation through membranes consisting of vertically-aligned double-walled carbon nanotube arrays. Carbon **146**, 785–788 (2019). https://doi.org/10.1016/j.carbon.2019.02.031
54. Q. Liu, L. Wen, K. Xiao, H. Lu, Z. Zhang, G. Xie, X.-Y. Kong, Z. Bo, L. Jiang, A biomimetic voltage-gated chloride nanochannel. Adv. Mater. **28**(16), 3181–3186 (2016). https://doi.org/10.1002/adma.201505250
55. L. Cao, F. Xiao, Y. Feng, W. Zhu, W. Geng, J. Yang, X. Zhang, N. Li, W. Guo, L. Jiang, Anomalous channel-length dependence in nanofluidic osmotic energy conversion. Adv. Mater. **27**(9), 1604302 (2017). https://doi.org/10.1002/adfm.201604302
56. J. Tang, Y. Wang, H. Yang, Q. Zhang, C. Wang, L. Li, Z. Zheng, Y. Jin, H. Wang, Y. Gu, T. Zuo, All-natural 2D nanofluidics as highly-efficient osmotic energy generators. Nat. Commun. **15**(1), 3649 (2024). https://doi.org/10.1038/s41467-024-47915-z
57. J. Liu, C. Li, P. Jia, J. Hao, L. Gao, J. Wang, L. Jiang, Large-Scale, Vertically aligned 2D subnanochannel arrays by a smectic liquid crystal network for high-performance osmotic energy conversion. Nat. Commun. (2024). https://doi.org/10.1002/adma.202313695
58. L. Chang, X. Xiao, The review of MXenes for osmotic energy harvesting: synthesis and properties. Diam. Relat. Mater. **136**, 109971 (2023). https://doi.org/10.1016/j.diamond.2023.109971
59. X. Tian, Y. Zhang, R. Zheng, D. Wei, J. Liu, Two-dimensional organic–inorganic hybrid Ruddlesden-Popper perovskite materials: preparation, enhanced stability, and applications in photodetection. Sustain. Energy Fuels **4**(5), 2087–2113 (2020). https://doi.org/10.1039/C9SE01181A
60. K. Li, W. Shen, T. Xu, L. Yang, X. Xu, F. Yang, L. Zhang, Y. Wang, Y. Zhou, M. Zhong, D. Wei, Fibrous gel polymer electrolyte for an ultrastable and highly safe flexible lithium-ion battery in a wide temperature range. Sustain. Energy Fuels **3**(6), 916–928 (2021). https://doi.org/10.1002/cey2.151
61. R. Qu, X. Zeng, L. Lin, G. Zhang, F. Liu, C. Wang, S. Ma, C. Liu, H. Miao, L. Cao, Vertically-oriented $Ti_3C_2T_x$ MXene membranes for high performance of electrokinetic energy conversion. ACS Nano **14**(12), 16654–16662 (2020). https://doi.org/10.1021/acsnano.0c02202
62. Z. Zhang, W. Shen, L. Lin, M. Wang, N. Li, Z. Zheng, F. Liu, L. Cao, Vertically transported graphene oxide for high-performance osmotic energy conversion. ACS Nano **7**(12), 2000286 (2020). https://doi.org/10.1002/advs.202000286
63. J. Ji, Q. Kang, Y. Zhou, Y. Feng, X. Chen, J. Yuan, W. Guo, Y. Wei, L. Jiang, Osmotic power generation with positively and negatively charged 2D nanofluidic membrane pairs. Adv. Sci. **27**(2), 1603623 (2017). https://doi.org/10.1002/adfm.201603623
64. L. Ding, D. Xiao, Z. Lu, J. Deng, Y. Wei, J. Caro, H. Wang, Oppositely charged $Ti_3C_2T_x$ MXene membranes with 2D nanofluidic channels for osmotic energy harvesting. Adv. Funct. Mater. **59**(22), 8720–8726 (2020). https://doi.org/10.1002/anie.201915993
65. L. Ding, M. Zheng, D. Xiao, Z. Zhao, J. Xue, S. Zhang, J. Caro, H. Wang, Bioinspired $Ti_3C_2T_x$ MXene-based ionic diode membrane for high-efficient osmotic energy conversion. Angew. Chem. Int. Ed. **61**(41), e202206152 (2022). https://doi.org/10.1002/anie.202206152
66. Y. Wu, W. Xin, X.-Y. Kong, J. Chen, Y. Qian, Y. Sun, X. Zhao, W. Chen, L. Jiang, L. Wen, Enhanced ion transport by graphene oxide/cellulose nanofibers assembled membranes for high-performance osmotic energy harvesting. Mater. Horiz. **7**(10), 2702–2709 (2020). https://doi.org/10.1039/D0MH00979B
67. D. Wang, Z. Wang, J. Chen, H. Zhi, Y. Liu, J. Tang, N. Li, Y. Zhang, M. An, H. Liu, G. Xue, Low-friction graphene oxide-based ion selective membrane for high-efficiency osmotic energy harvesting. Mater. Horiz. **14**(3), 2302262 (2024). https://doi.org/10.1002/aenm.202302262
68. R. Duan, J. Zhou, X. Ma, J. Hao, D. Zhao, C. Teng, Y. Zhou, L. Jiang, High strength MXene/PBONF heterogeneous membrane with excellent ion selectivity for efficient osmotic energy conversion. Nano Lett. **23**(23), 11043–11050 (2023). https://doi.org/10.1021/acs.nanolett.3c03343
69. D. Wei, M.R. Astley, N. Harris, R. White, T. Ryhänen, J. Kivioja, Graphene nanoarchitecture in batteries. Nanoscale **6**(16), 9536–9540 (2014). https://doi.org/10.1039/C4NR02089H
70. F. Wang, Z. Wang, S. Wang, X. Meng, Y. Jin, N. Yang, J. Sunarso, S. Liu, Mechanically intensified and stabilized MXene membranes via the combination of graphene oxide for highly efficient osmotic power production. J. Membrane Sci. **647**, 120280 (2022). https://doi.org/10.1016/j.memsci.2022.120280
71. H. Ouyang, X. Hong, Z. Zhou, P. Xu, H. Tang, Z. Ma, Z. Wang, X. Liao, L. He, Facile preparation of a MXene–graphene oxide membrane and its voltage-gated ion transport behavior. Phys. Chem. Chem. Phys. **24**(44), 27157–27162 (2022). https://doi.org/10.1039/D2CP03867F
72. J. Tian, A. Zhang, R. Liu, W. Huang, Z. Yuan, R. Zheng, D. Wei, J. Liu, Preparation of CoS_2 supported flower-like NiFe layered double hydroxides nanospheres for high-performance supercapacitors. J. Colloid Interf. Sci. **579**, 607–618 (2020). https://doi.org/10.1016/j.jcis.2020.06.086
73. W. Zhao, G. Yan, Y. Zheng, B. Liu, D. Jia, T. Liu, L. Cui, R. Zheng, D. Wei, J. Liu, Bimetal-organic framework derived $Cu(NiCo)_2S_4/Ni_3S_4$ electrode material with hierarchical hollow heterostructure for high performance energy storage. J. Colloid Interf. Sci. **565**, 295–304 (2020). https://doi.org/10.1016/j.jcis.2020.01.049
74. D. Wei, J.K. Baral, R. Österbacka, A. Ivaska, Electrochemical fabrication of a nonvolatile memory device based on polyaniline and gold particles. J. Mater. Chem. **18**(16), 1853–1857 (2008). https://doi.org/10.1039/B718227A
75. P. Peng, F. Yang, X. Li, S. Li, Z. Wang, D. Wei, High-power iontronics enabled by nanoconfined ion dynamics. Cell Rep. Phys. Sci. **5**(2), 101824 (2024). https://doi.org/10.1016/j.xcrp.2024.101824
76. F. Yang, P. Peng, Z.-Y. Yan, H. Fan, X. Li, S. Li, H. Liu, T.-L. Ren, Y. Zhou, Z.L. Wang, D. Wei, Vertical iontronic energy storage based on osmotic effects and electrode redox reactions. Nat. Energy **9**(3), 263–271 (2024). https://doi.org/10.1038/s41560-023-01431-4

77. D. Wei, D. Cotton, T. Ryhänen, All-solid-state textile batteries made from nano-emulsion conducting polymer inks for wearable electronics. Nanomaterials **2**(3), 268–274 (2012)
78. P. Peng, F. Yang, Z. Wang, D. Wei, Integratable Paper-based iontronic power source for all-in-one disposable electronics. Adv. Energy Mater. **13**(42), 2302360 (2023). https://doi.org/10.1002/aenm.202302360
79. J. Safaei, Y. Gao, M. Hosseinpour, X. Zhang, Y. Sun, X. Tang, Z. Zhang, S. Wang, X. Guo, Y. Wang, Z. Chen, D. Zhou, F. Kang, L. Jiang, G. Wang, Vacancy engineering for high-efficiency nanofluidic osmotic energy generation. J. Am. Chem. Soc. **145**(4), 2669–2678 (2023). https://doi.org/10.1021/jacs.2c12936
80. L. Cao, H. Wu, C. Fan, Z. Zhang, B. Shi, P. Yang, M. Qiu, N.A. Khan, Z. Jiang, Lamellar porous vermiculite membranes for boosting nanofluidic osmotic energy conversion. J. Mater. Chem. A **9**(25), 14576–14581 (2021). https://doi.org/10.1039/D1TA02400K
81. H. Qin, H. Wu, S.-M. Zeng, F. Yi, S.-Y. Qin, Y. Sun, L. Ding, H. Wang, Harvesting osmotic energy from proton gradients enabled by two-dimensional $Ti_3C_2T_x$ MXene membranes. Adv. Membr. **2**, 100046 (2022). https://doi.org/10.1016/j.advmem.2022.100046
82. P. Jia, X. Du, R. Chen, J. Zhou, M. Agostini, J. Sun, L. Xiao, The combination of 2D layered graphene oxide and 3D porous cellulose heterogeneous membranes for nanofluidic osmotic power generation. Molecules **26**(17), 5343 (2021). https://doi.org/10.3390/molecules26175343
83. J. Hao, Y. Wang, Y. Ning, X. Fan, J. Jiang, S. Meng, L. Chang, S. Hu, Y. Chen, X. Sui, Improved ion transfer and osmotic energy conversion via nanofibers/polymer composite membrane with hierarchical 3D porous. J. Power. Sources **604**, 234498 (2024). https://doi.org/10.1016/j.jpowsour.2024.234498
84. T. Lin, L. Zhang, C. Li, Y.-H. Fu, L. Gao, J.-L. Hou, Flexible organic framework-modified membranes for osmotic energy harvesting. Chinese J. Chem. **41**(14), 1713–1719 (2023). https://doi.org/10.1002/cjoc.202300012
85. J. Hao, B. Bao, J. Zhou, Y. Cui, X. Chen, J. Zhou, Y. Zhou, L. Jiang, A euryhaline-fish-inspired salinity self-adaptive nanofluidic diode leads to high-performance blue energy harvesters. Adv. Mater. **34**(31), 2203109 (2022). https://doi.org/10.1002/adma.202203109
86. J. Chmiola, G. Yushin, Y. Gogotsi, C. Portet, P. Simon, P.L. Taberna, Anomalous increase in carbon capacitance at pore sizes less than 1 nanometer. Science **313**(5794), 1760–1763 (2006). https://doi.org/10.1126/science.1132195
87. M.R. Lukatskaya, S. Kota, Z. Lin, M.-Q. Zhao, N. Shpigel, M.D. Levi, J. Halim, P.-L. Taberna, M.W. Barsoum, P. Simon, Y. Gogotsi, Ultra-high-rate pseudocapacitive energy storage in two-dimensional transition metal carbides. Nat. Energy **2**(8), 17105 (2017). https://doi.org/10.1038/nenergy.2017.105
88. R. Fan, S. Huh, R. Yan, J. Arnold, P. Yang, Gated proton transport in aligned mesoporous silica films. Nat. Mater. **7**(4), 303–307 (2008). https://doi.org/10.1038/nmat2127
89. B. Yao, S. Hussain, Z. Ye, X. Peng, Electrodeposited MOFs Membrane with in situ incorporation of charged molecules for osmotic energy harvesting. Small **19**(18), 2207559 (2023). https://doi.org/10.1002/smll.202207559
90. S. Aghapour Aktij, M. Dadashi Firouzjaei, S.A. Haddadi, P. Karami, A. Taghipour, M. Yassari, A.A. Asad, M. Pilevar, H. Jafarian, M. Arjmand, M. Elliott, A. Rahimpour, J.B.P. Soares, M. Sadrzadeh, Metal-organic frameworks' latent potential as high-efficiency osmotic power generators in thin-film nanocomposite membranes. Chem. Eng. J. **481**, 148384 (2024). https://doi.org/10.1016/j.cej.2023.148384
91. J. Zhou, J. Hao, R. Wu, L. Su, J. Wang, M. Qiu, B. Bao, C. Ning, C. Teng, Y. Zhou, L. Jiang, Maximizing ion permselectivity in MXene/MOF nanofluidic membranes for high-efficient blue energy generation. Adv. Funct. Mater. **32**(49), 2209767 (2022). https://doi.org/10.1002/adfm.202209767
92. W. Fu, J. Zhang, Q. Zhang, M. Ahmad, Z. Sun, Z. Li, Y. Zhu, Y. Zhou, S. Wang, Construction of metal-organic framework/cellulose nanofibers-based hybrid membranes and their ion transport property for efficient osmotic energy conversion. Int. J. Biol. Macromol. **257**, 128546 (2024). https://doi.org/10.1016/j.ijbiomac.2023.128546
93. J. Xiao, M. Cong, M. Li, X. Zhang, Y. Zhang, X. Zhao, W. Lu, Z. Guo, X. Liang, G. Qing, Self-assembled nanoporous metal–organic framework monolayer film for osmotic energy harvesting. Adv. Funct. Mater. **34**(2), 2307996 (2024). https://doi.org/10.1002/adfm.202307996
94. Y. Liu, Y. Chen, Y. Guo, X. Wang, S. Ding, X. Sun, H. Wang, Y. Zhu, L. Jiang, Photo-controllable ion-gated metal–organic framework MIL-53 Sub-nanochannels for efficient osmotic energy generation. ACS Nano **16**(10), 16343–16352 (2022). https://doi.org/10.1021/acsnano.2c05498
95. R.K. Tonnah, M. Chai, M. Abdollahzadeh, H. Xiao, M. Mohammad, E. Hosseini, M. Zakertabrizi, D. Jarrahbashi, A. Asadi, A. Razmjou, M. Asadnia, Bioinspired angstrom-scale heterogeneous MOF-on-MOF membrane for osmotic energy harvesting. ACS Nano **17**(13), 12445–12457 (2023). https://doi.org/10.1021/acsnano.3c01924
96. C. Wang, J. Tang, L. Li, J. Wan, Y. Ma, Y. Jin, J. Liu, H. Wang, Q. Zhang, Ultrathin self-standing covalent organic frameworks toward highly-efficient nanofluidic osmotic energy generator. Adv. Funct. Mater. **32**(36), 2204068 (2022). https://doi.org/10.1002/adfm.202204068
97. R. Li, J. Zhai, J. Jiang, Q. Wang, S. Wang, Improved interfacial ion transport through nanofluidic hybrid membranes based on covalent organic frameworks for osmotic energy generation. ACS Appl. Energy Mater. **5**(6), 7176–7184 (2022). https://doi.org/10.1021/acsaem.2c00734
98. Z. Man, J. Safaei, Z. Zhang, Y. Wang, D. Zhou, P. Li, X. Zhang, L. Jiang, G. Wang, Serosa-simetic nanoarchitecture membranes for highly efficient osmotic energy generation. J. Am. Chem. Soc. **143**(39), 16206–16216 (2021). https://doi.org/10.1021/jacs.1c07392
99. L. Cao, I.C. Chen, X. Liu, Z. Li, Z. Zhou, Z. Lai, An ionic diode covalent organic framework membrane for efficient osmotic energy conversion. ACS Nano **16**(11), 18910–18920 (2022). https://doi.org/10.1021/acsnano.2c07813
100. X. Zuo, C. Zhu, W. Xian, Q.-W. Meng, Q. Guo, X. Zhu, S. Wang, Y. Wang, S. Ma, Q. Sun, Thermo-osmotic energy conversion enabled by covalent-organic-framework membranes with record output power density. Angew. Chem. Int. Ed. **61**(18), e202116910 (2022). https://doi.org/10.1002/anie.202116910
101. X. Zhao, P. Pachfule, A. Thomas, Covalent organic frameworks (COFs) for electrochemical applications. Chem. Soc. Rev. **50**(12), 6871–6913 (2021). https://doi.org/10.1039/D0CS01569E
102. M. Gao, P.-C. Tsai, Y.-S. Su, P.-H. Peng, L.-H. Yeh, Single mesopores with high surface charges as ultrahigh performance osmotic power generators. Small **16**(48), 2006013 (2020). https://doi.org/10.1002/smll.202006013
103. J.-P. Hsu, T.-C. Su, P.-H. Peng, S.-C. Hsu, M.-J. Zheng, L.-H. Yeh, Unraveling the anomalous surface-charge-dependent osmotic power using a single funnel-shaped nanochannel. ACS Nano **13**(11), 13374–13381 (2019). https://doi.org/10.1021/acsnano.9b06774
104. J. Hao, S. Ma, Y. Hou, W. Wang, X. Dai, X. Sui, Concise and efficient asymmetric homogeneous Janus membrane for high-performance osmotic energy conversion based on oppositely charged montmorillonite. Electrochim. Acta **423**, 140581 (2022). https://doi.org/10.1016/j.electacta.2022.140581
105. Y. Sun, T. Dong, C. Lu, W. Xin, L. Yang, P. Liu, Y. Qian, Y. Zhao, X.-Y. Kong, L. Wen, L. Jiang, Tailoring a poly(ether sulfone) bipolar membrane: osmotic-energy generator with high power density. Angew. Chem. Int. Ed. **59**(40), 17423–17428 (2020). https://doi.org/10.1002/anie.202006320

106. J. Chen, W. Xin, X.-Y. Kong, Y. Qian, X. Zhao, W. Chen, Y. Sun, Y. Wu, L. Jiang, L. Wen, Ultrathin and robust silk fibroin membrane for high-performance osmotic energy conversion. ACS Energy Lett. **5**(3), 742–748 (2020). https://doi.org/10.1021/acsenergylett.9b02296
107. P. Ramírez, P.Y. Apel, J. Cervera, S. Mafé, Pore structure and function of synthetic nanopores with fixed charges: tip shape and rectification properties. Nanotechnology **19**(31), 315707 (2008). https://doi.org/10.1088/0957-4484/19/31/315707
108. G. Laucirica, A.G. Albesa, M.E. Toimil-Molares, C. Trautmann, W.A. Marmisollé, O. Azzaroni, Shape matters: enhanced osmotic energy harvesting in bullet-shaped nanochannels. Nano Energy **71**, 104612 (2020). https://doi.org/10.1016/j.nanoen.2020.104612
109. J. Lu, H. Xu, H. Yu, X. Hu, J. Xia, Y. Zhu, F. Wang, H.-A. Wu, L. Jiang, H. Wang, Ultrafast rectifying counter-directional transport of proton and metal ions in metal-organic framework–based nanochannels. Sci. Adv. **8**(14), eabll5070 (2022). https://doi.org/10.1126/sciadv.abl5070
110. D. Wei, T. Lindfors, C. Kvarnström, L. Kronberg, R. Sjöholm, A. Ivaska, Electrosynthesis and characterisation of poly(N-methylaniline) in organic solvents. J. Electroanal. Chem. **575**(1), 19–26 (2005). https://doi.org/10.1016/j.jelechem.2004.08.018
111. Q. Ren, H. Hu, Q. Zeng, Q. Jiang, P. Wang, Hybrid solar photovoltaic and salinity-gradient based osmotic energy conversion system with synergistic performance enhancement. Energ. Convers. Manag. **283**, 116898 (2023). https://doi.org/10.1016/j.enconman.2023.116898
112. N. Kutlu, Optimization of ohmic heating-assisted osmotic dehydration as a pretreatment for microwave drying of quince. Food Sci. Technol. Int. **28**(1), 60–71 (2022). https://doi.org/10.1177/1082013221991613
113. L. Chang, T. Zhang, F. Wang, H. Ma, W. Xie, T. Ding, X. Xiao, Cation-selective $Mo_2TiC_2T_x$ MXene membrane for osmotic energy harvesting. 2D Materials **10**(1), 014009 (2023). https://doi.org/10.1088/2053-1583/ac9ceb
114. F. Yi, H. Ren, K. Dai, X. Wang, Y. Han, K. Wang, K. Li, B. Guan, J. Wang, M. Tang, J. Shan, H. Yang, M. Zheng, Z. You, D. Wei, Z. Liu, Solar thermal-driven capacitance enhancement of supercapacitors. Energy Environ. Sci. **11**(8), 2016–2024 (2018). https://doi.org/10.1039/C8EE01244J
115. H. Yang, H. Fang, W. Wang, D. Zhang, J. Zhu, K. Chen, Y. Sun, P. Wang, Q. Zhou, C. Qi, B. Wang, M. Wu, 3D printing of flexible batteries for wearable electronics. J. Power. Sources **602**, 234350 (2024). https://doi.org/10.1016/j.jpowsour.2024.234350
116. X. Lin, Y. Dong, S. Tao, X. Feng, X. Wang, T. Song, J. Liu, Z. Zhong, Y. Wang, H. Qi, Temperature-gated nanocellulose membrane for enhanced and controllable osmotic energy harvesting. Nano Energy **107**, 108156 (2023). https://doi.org/10.1016/j.nanoen.2022.108156
117. Y. Ouyang, X. Li, S. Li, P. Peng, F. Yang, Z.L. Wang, D. Wei, Opto-iontronic coupling in triboelectric nanogenerator. Nano Energy **116**, 108796 (2023). https://doi.org/10.1016/j.nanoen.2023.108796
118. Q. Wang, Y. Wu, C. Zhu, Y. Hu, L. Fu, Y. Qian, Z.-H. Zhang, T. Li, X. Li, X.-Y. Kong, L. Jiang, Z. Zhang, L. Wen, Efficient solar-osmotic power generation from bioinspired anti-fouling 2D WS_2 composite membranes. Angew. Chem. Int. Ed. **62**(23), e202302938 (2023). https://doi.org/10.1002/anie.202302938
119. Z.-Q. Li, G.-L. Zhu, R.-J. Mo, M.-Y. Wu, X.-L. Ding, L.-Q. Huang, Z.-Q. Wu, X.-H. Xia, Light-enhanced osmotic energy harvester using photoactive porphyrin metal–organic framework membranes. Angew. Chem. Int. Ed. **61**(22), e202202698 (2022). https://doi.org/10.1002/anie.202202698
120. J. Cai, J. Zhao, X. Gao, W. Ma, D. Meng, H. Zhang, C. Hao, M. Sun, H. Kuang, C. Xu, L. Xu, Magnetic field tuning ionic current generated by chiromagnetic nanofilms. ACS Nano **16**(7), 11066–11075 (2022). https://doi.org/10.1021/acsnano.2c03778
121. J. Pu, H. Zhu, Q. Wang, Z. Qu, J. Zhang, Bifunctional device for osmotic energy conversion and photothermal water evaporation enabled by synergy of salinity and pressure gradients with thermal assistance. ACS Energy Lett. **9**(5), 2410–2419 (2024). https://doi.org/10.1021/acsenergylett.4c00372